Chapter 4

ELECTROCHEMICAL TREATMENT OF HUMAN WASTE COUPLED WITH MOLECULAR HYDROGEN PRODUCTION

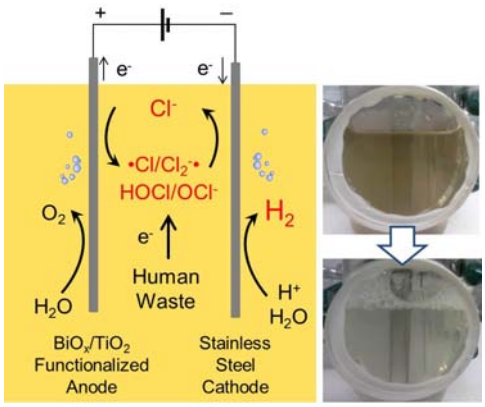

Sections reprinted with permission from Kangwoo Cho, Daejung Kwon, and Michael R. Hoffmann *RSC Advances* **2014**, *4*, 4596-4608.

ABSTRACT

We have developed a wastewater treatment system that incorporates an electrolysis cell for on-site wastewater treatment coupled with molecular hydrogen production for use in a hydrogen fuel cell. Herein, we report on the efficacy of a laboratory-scale wastewater electrolysis cell (WEC) using real human waste for the first time with a semiconductor electrode utilizing a mixed particle coating of bismuth oxide doped titanium dioxide (BiO_x/TiO_2). A comprehensive environmental analysis has been coupled together with a robust kinetic model under the chemical reaction limited regime to investigate the role of various redox reactions mediated by chloride present in human waste. The oxidative elimination of the *chemical oxygen demand* (COD) and ammonium ion can be modelled using empirical, pseudo-first-order rate constants and current efficiencies (CE). In combination with an anaerobic pre-treatment step, human waste containing high-levels of COD, protein, and color are eliminated within 6 h of batch treatment in the WEC. The reactor effluent has residual inorganic total nitrogen (TN) concentration of ~ 40 mM. The CE and specific energy consumption were 8.5% and 200 kWh $kgCOD^{-1}$ for the COD removal, 11% and 260 for kWh $kgTN^{-1}$ for the TN conversion. The CE and energy efficiencies (EE) for hydrogen production were calculated to be 90% and 25%, respectively.

4.1. INTRODUCTION

There has been an increasing awareness of an emerging crisis with respect to water resources due to global population growth and climate change. Close to 80% of the world's population is threatened by water scarcity, due primarily to a deficit of safe drinking water and water for personal sanitation.[1] It is estimated that 2.7 billion people lack access to sufficient water for human sanitation (*i.e.*, for personal hygiene) and proper waste disposal.[2] The direct discharge of untreated human waste and open defecation are major sources of waterborne diseases. Furthermore, the biochemical oxygen demand (BOD) generated by the discharge of human waste into receiving waters is becoming a threat to biodiversity. As a consequence, research has been focused on approaches to enhance the water safety and productivity for non-consumptive uses by technological improvement in wastewater treatment and reuse practices.[2,3] However, a lack of infrastructures in the developing world and highly interrelated water-energy nexus[3] require the water treatment and reuse practices to be on-site, energy sustainable, and economical with a minimal use of hydraulic retention time (HRT) and material costs.

In order to address some of these problems, we are exploring the use of electrochemical reactors or wastewater electrolysis cells (WEC) that have been designed to provide on-site wastewater treatment for water recycling and reuse coupled with energy storage. Electrochemical water oxidation to oxygen on metal oxides anodes is known to initiate by formation of surficial hydroxyl radicals and/or by direct electron transfer to surface-bound holes,[4-6] which can be used for the 'direct' oxidation of environmental contaminants. Wastewater with a sufficient level of electrical conductivity

(σ), such as dye wastewater and landfill leachate, has been investigated extensively for the electrochemical removal of pollutants.[4,6] The near ubiquitous presence of chloride (Cl^-) in the high-salinity wastewater often leads to the homogeneous 'indirect' oxidation via production of reactive chlorine species (RCS) including free chlorine (Cl_2, HOCl, ClO^-)[4,6] and chlorine radicals ($Cl\cdot$, $Cl_2^-\cdot$).[7] The existence of chloride has been frequently reported to reduce specific energy consumption (SEC) for electrochemical oxidation of chemical pollutants by increasing σ and substrate degradation rates at a given current (or potential).[8-14]

Energy conversion and storage are possible due to electron transfer to water or proton to produce hydrogen at the cathodes. This can lead to a much lower carbon footprint when compared to the steam reformation of methane to produce hydrogen.[7,15,16] Under a sufficient solar irradiation, the WEC can be powered by an appropriate size of photovoltaic (PV) panels,[7,15,17-19] to allow for a sustainable and traditional-infrastructure-free approach to human waste treatment coupled with the generation of an energy-rich by-product (*e.g.*, H_2). Therefore, a PV-powered WEC (PWEC) has the potential to address the global needs for energy, water, and human health by using green chemistry without additional chemical reagents (*e.g.*, O_3, H_2O_2, $S_2O_8^{2-}$, etc.) to achieve a high-degree of BOD reduction.

It is possible to achieve energy efficient hydrogen production[20] coupled with chemical contaminant oxidation[21,22] when utilizing electrochemically active anodes with high oxygen evolution reaction (OER) rates. Intrinsic cost-effectiveness and mechanical/chemical inertness are also important considerations for the proper design of

electrodes.[5,20] Electrodes with high OER overpotentials (η), based on SnO_2, PbO_2, and BDD (Boron Doped Diamond), have been used exclusively for the direct electrochemical oxidation.[4,6,23] In spite of superior current efficiencies for organic compound oxidation, these electrodes would not be suitable for energy conversion due to the lack of electrocatalytic activity and large energy losses.[21,22] Facile O_2/Cl_2 evolution at active novel Pt group metal oxides (RuO_2 and IrO_2) and combined usage with inert metal oxides (TiO_2, Ta_2O_5, and SnO_2) to increase corrosion resistance allowed their applications for water splitting, chlor-alkali production, and wastewater electrooxidation.[5,20,24,25] However, the high material cost of low-abundance metals (*i.e.*, Ru and Ir) is a major limitation for their commercial application.[20] The electrocatalytic OER activity has long been ascribed to a reversible redox transition within the potential energy window of water splitting.[5,20] In this regard, the pseudo-capacitance and dielectric permittivity of Bi_2O_3 provide a less costly approach for OER systems and for use in Faradaic supercapacitors.[26] Accelerated ion conductivity due to the intrinsic (disordered) oxygen vacancies and high polarizability due to the presence of $6s^2$ lone pair in Bi enables Bi_2O_3 to be applied as a solid oxide fuel cell electrolyte.[27] Based on the promising characteristics of this earth abundant metal oxide, our previous reports[7,15,16,18,19] have demonstrated the feasibility of Bi-doped TiO_2 (BiO_x/TiO_2) electrodes for use in the WEC.

Herein, we report on the efficacy of the WEC equipped with the BiO_x/TiO_2 anode as a novel, dual-functioning approach for treatment and/or reuse of liquid human waste coupled with the simultaneous production of molecular hydrogen. Human urine is often a source of chloride present in domestic wastewater, which in turn can be oxidized to RCS, resulting in further organic compound oxidation and disinfection. The complex reaction

network involved in chloride mediated indirect oxidation[4,6] and the large number of operational variables that include current, applied cell voltage, pre-treatment, influent dilution, fluid-flow, and mixing[28] require reliable kinetic models in order to explore the role of each operational parameter. Consistent with the electrocatalytic behavior of our BiO_x/TiO_2 composite electrodes, a simple kinetic model is derived based on the measured rate constants for pollutant degradation, current efficiency, and specific energy consumption.

4. 2. EXPERMIENTAL SECTION

4.2.1. BiO_x/TiO_2 Electrode Preparation. The multi-layered semiconductor electrodes were prepared by sequential deposition of mixed metal oxides[29] as follows: (i) an anti-passivation layer of IrO_2/Ta_2O_5 with a molar ratio of 73:27 (Ir:Ta), (ii) a sealing coat of SnO_2/Bi_2O_3 at Sn:Bi of 9:1, (iii) a slurry deposition of bismuth oxide doped TiO_2 (BiO_x/TiO_2) nanoparticles with Bi:Ti of 1:24, and (iv) BiO_x/TiO_2 thin film (over-coat) deposition at a molar ratio of 1:2 (Bi:Ti). Each thermal decomposition procedure requires a specific precursor composition, heat treatment, and repetition as described in the Supporting Information. In a recent report, we showed that the electrodes as prepared are dominated by the elemental composition of Ti, Bi, and O in electrochemically active outermost surface;[18] thus we will refer to our composite anodes as BiO_x/TiO_2 electrode. The anti-passivation layer together with the sealing coat is known to enhance the robustness and electric conductivity.[29]

4.2.2. Electrochemical Setup. The electrode modules used in this study consisted of a BiO_x/TiO_2 anode, a stainless steel (SS, Hastelloy C-22) cathode, and an

Ag/AgCl/Saturated KCl reference electrode (BaSi Inc., USA). The effective area of the anode and cathode was 5.4 cm^2 (2.7 cm × 2 cm). The distance between anode and cathode was 5 mm, while the reference electrode was located as close as possible to the anode. Hereafter, the electrochemical potentials are always expressed in terms of the normal hydrogen electrode (NHE). The electrochemical cells were powered by a potentiostat (SP-50, Bio-Logic, France) in which the applied anodic potential (E_a) was adjusted with continuous monitoring of the response current (i) and cathodic potential (E_c).

4.2.3. Electrode Characterization. The cyclic voltammetry (CV) data were collected using either a 50 mM NaCl or a 50 mM $NaClO_4$ electrolyte solution under quiescent conditions for three cycles consecutively without open-circuit resting. The scan rate and scan range were fixed at 5 mV sec^{-1} and 0 – 3 V, respectively. The chrono-amperometric data were collected in stirred solutions with 10, 30, and 50 mM NaCl, where the E_a was varied from 1.5 to 3.5 V in 0.5 V increments. The resulting data were stored for 10 min at each E_a while resting the system in an open circuit for 5 min before adjustment of each potential increment. The CV and chrono-amperometric experiments were performed in a single compartment cell with working volume of 275 mL. In order to assess the direct oxidation efficacy of the BiO_x/TiO_2 electrode, a bulk potentiostatic electrolysis (E_a: 3 V) was performed in 47.5 mL KH_2PO_4 solution (5.3 mM), whose small fraction (2 mL) was sequentially replaced with 10 mM NaCOOH solution in 10 min intervals without a change in σ. The variations in I and $[HCO_2^-]$ were monitored as functions of electrolysis time.

4.2.4. Wastewater Sample Preparation. Table 4.1 shows the average composition of urine collected from an Asian male (Age: 30) and domestic wastewater (DWW). The DWW was obtained at San Jose Creek Wastewater Treatment facility (tertiary treatment) operated by the Sanitation Districts of Los Angeles County (USA). Samples were collected after a primary settling tank and stored in 4 ºC before usage.

To simulate septic tank effluents (STEs), the urine was mixed with the DWW with a volumetric ratio of 1:3 and anaerobically incubated at 35 °C for 2 days (conventional HRT in septic tanks[30]). Under these conditions, the high-molecular-weight organic compounds in urine can be biodegraded into lower molecular weight fragments by the microorganisms present in wastewater. Pre-treated urine was further diluted with the DWW with the mixing ratio of 1:9 (STE1), 1:4 (STE2), and 1:1 (STE3), which produced

Table 4.1. Composition of the as-received domestic wastewater (DWW), urine, and model septic tank effluent (STE 1-4, see Supporting Information for details).

Constituent	DWW	Urine	STE1	STE2	STE3	STE4
pH	7.1	6.6	8.9	9.0	9.1	9.0
Conductivity (mS cm^{-1})	1.1	24	2.3	3.5	7.0	8.8
COD (mg L^{-1})	180	5300	310	480	900	460
TN (mM N)	2.6	410	13	25	61	66
Urea (mM)	< 0.01	159	2.4	1.1	5.8	7.4
NH_4^+ (mM)	1.9	21	12	24	38	44
NO_3^- (mM)	< 0.01	1.1	0.01	0.10	0.01	0.10
Cl^- (mM)	3.9	180	6.7	10	21	33
Protein (mg BSA L^{-1})	75	2300	160	250	520	280
Carbohydrate (mg glucose L^{-1})	35	530	16	39	63	23
Organic Acids (mM)	< 0.01	6.9	0.02	1.6	3.1	0.09

variable concentrations of mixed organic waste and chloride, as shown in Table 4.1. Since the microbial concentration in DWW should be much smaller than in a septic tank, digested urine after 7 days of incubation was also tested without further dilution (STE4).

4.2.5. WEC Experiments. The WEC setup consists of the electrode module in a single compartment electrolysis cell equipped with a side-branch sampling port and a gas outlet port on top. Initial working electrolyte and corresponding headspace volumes in the reactor were 55 mL and 20 mL, respectively. Potentiostatic electrolyses (E_a: 3 V) were performed in 30 and 50 mM NaCl solutions for 3 h to investigate the chloride oxidation kinetics in the absence of organic matter. The WEC experiments using urine (with and without dilution) and STEs proceeded for 6 h, again with constant E_a (3 V). Small aliquots of the electrolyte were collected for analyses without changing the working electrode surface area. During the middle (80 – 110 min) and the end phase (300 – 330 min) of the electrolyses, the sampling port was sealed with a rubber stopper for 30 min to introduce the headspace gas into a graded burette. The average total volumetric flow rate of gaseous products (Q) was monitored and the molar flow rate of hydrogen (F_{H2}) was scaled based on the volumetric fraction of hydrogen (X_{H2}), which was determined by a GC/TCD (Gas Chromatography with Thermal Conductivity Detector).

4.2.6. Chemical Analyses. The pH and conductivity were monitored using a Mettler Toledo EL20 pH meter and VWR portable conductivity meter. In order to determine the chemical oxygen demand (COD), samples were digested in a low range dichromate digestion solution (3 – 150 mg L^{-1}) in a COD reactor (DRB-200, Hach, USA) and quantified based on the absorbance at 420 nm. The total nitrogen (TN) concentration was

measured by the absorbance at 420 nm after treatment using a TN reagent set. Anions (Cl^-, ClO_3^-, NO_2^-, NO_3^-, HCO_2^-, $C_2O_4^{2-}$, $C_2H_3O_2^-$) and cations (NH_4^+, Na^+, Ca^{2+}, Mg^{2+}) were simultaneously determined by ion chromatography (DX-500, Dionex, USA) using an anion-exchange column Ionpac AS 19 and a cation-exchange column Ionpac CS 16. The protein and carbohydrate concentrations were measured using the Lowry method[31] and the phenol/sulfuric acid method.[32] The total chlorine (Cl_{DPD}) was measured using the DPD (N,N-diethyl-p-phenylenediamine) method at a wavelength of 530 nm. The concentration of urea was quantified based on the product ammonium concentration after hydrolysis with jack-bean urease. Absorbance measurements were made using an Agilent 8453 UV-VIS spectrophotometer.

4.3. RESULTS AND DISCUSSION

4.3.1. Voltammetric Characteristics of the WEC. The space-time extent of pollutant oxidation is generally expected to increase with the applied potential (or current) when the effects of the current density (J) on a desired current efficiency are not substantial.[28,33] However, concomitant augmentation of the solution resistance (iR) would be significant[34] in the WEC since the σ of electrolyte is much lower than in an industrial electrolyzer or chlor-alkali cell. Therefore, dealing with the WEC for energy conversion purposes, it is essential to investigate the variation of iR-compensated anodic potential ($E_a - iR$), J, and cell voltage ($E_a - E_c$) as a function of the E_a. As shown in Figure 4.1a, the iR sharply increases as the E_a increases due to the exponential dependence of i on the $E_a - iR$. The increase of $E_a - iR$ was marginal at an E_a above 3 V where additional power consumption should not contribute to the rate of electron transfer. Therefore, subsequent WEC

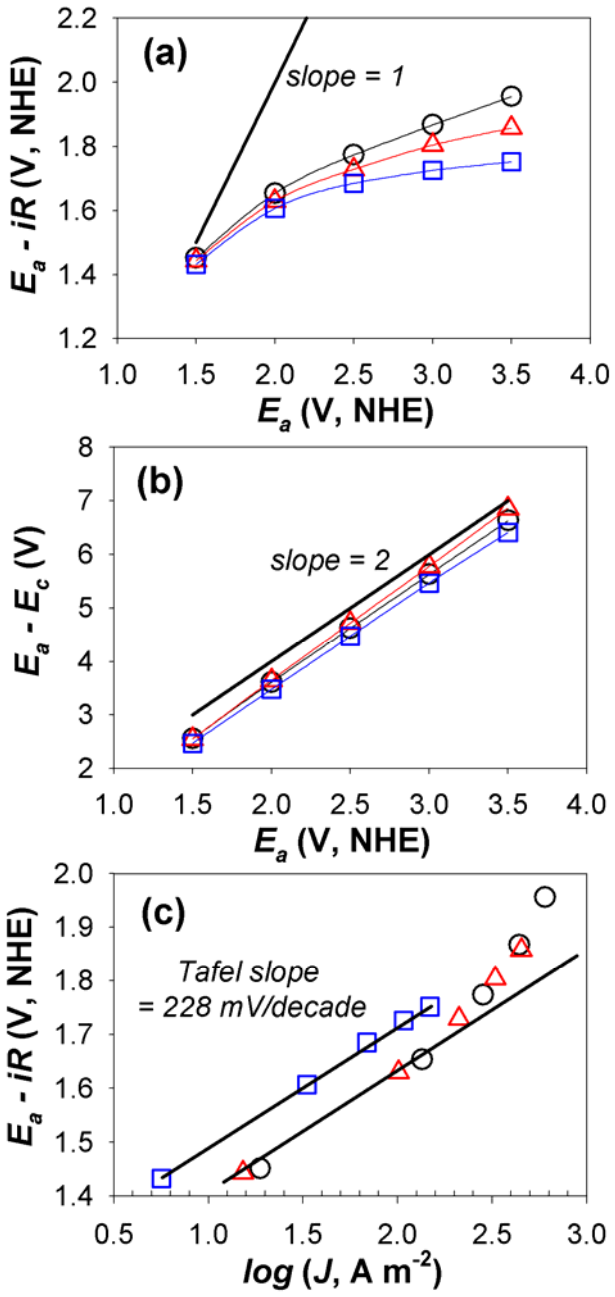

Figure 4.1. Dependence of (a) *iR* compensated anodic potential (E_a – iR) on applied anodic potential (E_a), (b) cell potential (E_a – E_c) on E_a, and (c) logarithmic current density (J) on the E_a – iR during chronoamperometric experiment in a single compartment electrolysis cell with 10 mM (square, R: 21.9 Ω), 30 mM (triangle, R: 6.8 Ω), and 50 mM (circle, R: 4.8 Ω) NaCl solution (275 mL).

experiments were carried out under potentiostatic conditions with the E_a of 3 V. The energy loss at high applied potentials should be emphasized considering that the $E_a - E_c$ is the actual determinant of the energy consumption; in this study, an equivalent magnitude of E_c was required to manipulate the E_a (Figure 4.1b).[33] This observation points out a potential problem, especially in dilute solution, with inferring that various reactive oxidants are present based on the cell voltage. For example, in 10 mM NaCl solution, the value of $E_a - iR$ at an $E_a - E_c$ of 6.41 V was only 1.75 V (27%), smaller than the thermodynamic potential required to form H_2O_2, O_3, as well as ·OH, Cl·, and Cl_2^{-}·. The reactive intermediates such as hydroxyl and chlorine radicals should be surface-bound to play a role without an $E_a - iR$ exceeding their redox potentials (E).

4.3.2. Electrochemistry of the BiO_x/TiO_2 Anode in Dilute Chloride Solutions. The BiO_x/TiO_2 has been used as a visible-light photocatalyst due to the characteristics of Bi_2O_3, including high refractive index and photoconductivity coupled with a relatively small band gap (~ 2.8 eV).[35] We also show that the BiO_x/TiO_2 anode is an excellent electrochemical catalyst for generation of oxygen and RCS. In Figure 4.2, we illustrate the cyclic voltammetry of the BiO_x/TiO_2 in 50 mM NaCl and 50 mM $NaClO_4$ solutions. The onset potential of the anodic wave was observed near 1.16 V (NHE) in both electrolytes; this corresponds to an OER η of 0.32 V. The OER η value of the BiO_x/TiO_2 is low compared with those of IrO_2 and RuO_2 based electrodes.[8,11,36] Since the OER η value is closely related to the enthalpy of oxide transition,[20] the facile OER activity of the BiO_x/TiO_2 anode can be attributed to the oxide ion conducting BiO_x rather than the electrochemically resistant TiO_2. According to Comninellis[23], the OER on metal oxides electrodes functions according to the following set of reactions:

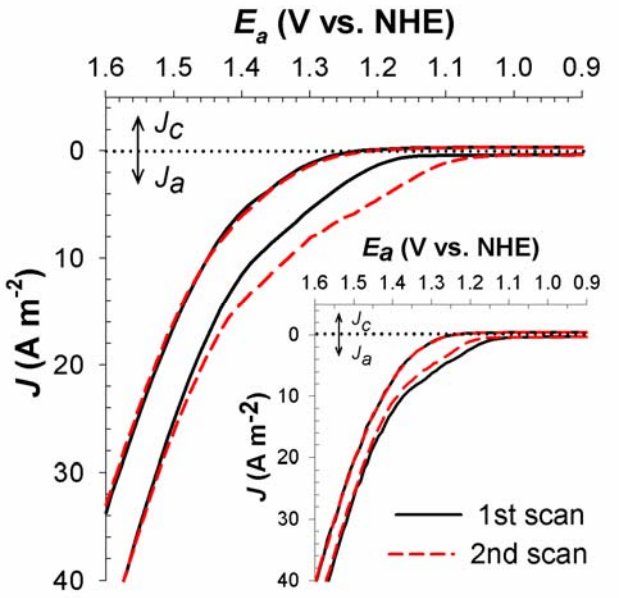

Figure 4.2. Cyclic voltammetry (CV) of a single compartment electrolysis cell with 50 mM NaCl (σ: 5.5 mS cm^{-1}, R: 4.5 Ω, pH: 6.6) or 50 mM $NaClO_4$ (inset, σ: 5.1 mS cm^{-1}, R: 4.6 Ω, pH: 6.6) solution (275 mL).

$$MO_x + H_2O \xrightarrow{k_1} MO_x(\cdot OH) + H^+ + e^- \quad (4.1)$$

$$MO_x(\cdot OH) \xrightarrow{k_2} MO_{x+1} + H^+ + e^- \quad (4.2)$$

$$MO_x(\cdot OH) \xrightarrow{k_{3a}} MO_x + 1/2\ O_2 + H^+ + e^- \quad (4.3a)$$

$$MO_{x+1} \xrightarrow{k_{3b}} MO_x + 1/2\ O_2 \quad (4.3b)$$

The physi-sorbed ($MO_x(\cdot OH)$) and chemi-sorbed (MO_{x+1}) active oxygen would in turn react with Cl^- to form the RCS, resulting in an indirect oxidation of environmental pollutants, while reactions of the $MO_x(\cdot OH)$ or surface-trapped holes with electron donors is often classified as direct oxidation.[4,6] The contribution of the surface bound hydroxyl radicals can be estimated by monitoring the current variation at a fixed E_a under

a sequential addition of an organic electron donor (*e.g.*, formate).[37] As shown in Figure 4.3, the measured formate concentration did not deviate from the stepwise increasing time profile (without degradation), while the current variation was marginal as well. Therefore, the $MO_x(\cdot OH)$ or the valence-band hole do not appear to be major contributors in oxidation pathways on the BiO_x/TiO_2 anode. The negligible heterogeneous surface degradation of formate might be partially attributed to a mass transport limitation to the anode surface. However, we propose that an internal oxidation of Bi(III) to the higher Bi(V) valence state would rapidly quench the $MO_x(\cdot OH)$. Figure 4.1c illustrates the chrono-amperometric current response in 10, 30, and 50 mM NaCl solutions. In a lower anodic potential region, the relationship between the log J and $E_a - iR$ was governed by a linear Tafel equation, with a slope of 228 mV decade^{-1} independent of the [Cl^-]. The magnitude of the Tafel slope, which has been used to elucidate the rate determining step (RDS) in a multi-step reaction sequence,[24,25,38] suggests that the formation of $MO_x(\cdot OH)$ (eq 4.1) would be the RDS with a charge transfer coefficient around 0.25. The α-phase Bi_2O_3 is known to have one quarter of an oxide vacancy per unit cell.[27] In addition, partial substitutions of Ti^{4+} with the effective ionic radius (r_{ion}) of 61 pm by Bi^{3+} with r_{ion} of 103 pm provide for additional oxide vacancies that are favorable to the III/V valence state transition.[35] The minor direct oxidation efficacy, which is related with oxygen deficiencies,[5] has been previously demonstrated for RuO_x/TiO_2 electrodes.[8,12,21,39]

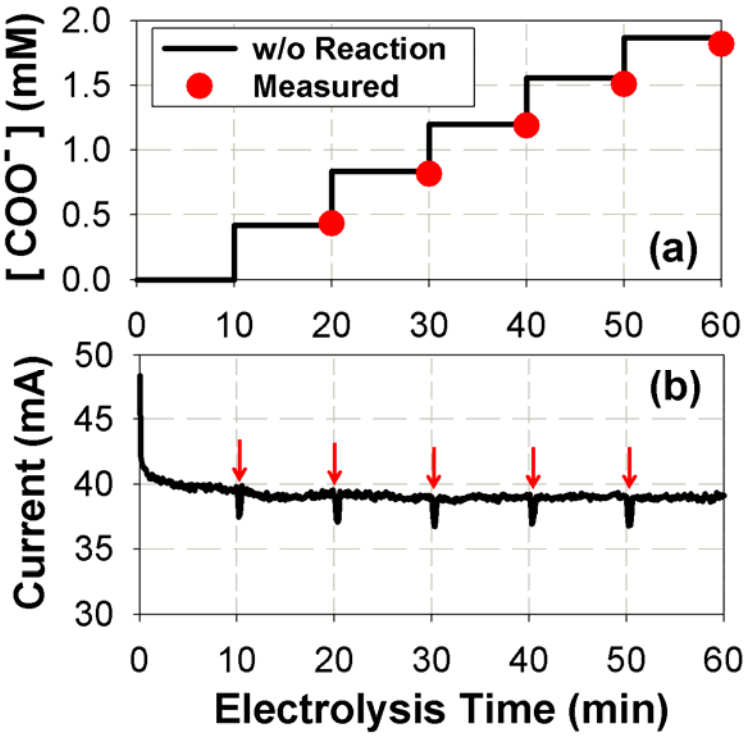

Figure 4.3. (a) Evolution of the formate concentration and (b) current variation under sequential substitution (2 mL, arrows) with 10 mM NaCOOH (σ: 0.92 mS/cm) in a potentiostatic (E_a: 3 V), single compartment electrolysis cell; initial electrolyte: 5.3 mM KH_2PO_4 47.5 mL (pH: 7.2, σ: 0.92 mS/cm).

Several possible reaction mechanisms for the chlorine evolution reaction (CER) on the RuO_2 or RuO_2/TiO_2 are consistent with the MO_{x+1} surface species as the dominant reactive site for chloride oxidation.[24,25,38] In a typical sequence, Cl^- is initially oxidized to a surface bound ClO^- (eq 4.4a), which in turn reacts with another chloride in bulk aqueous solution or on the electrode surface to produce Cl_2 (eq 4.4b). In addition, an $E_a - iR$ exceeding the E of $Cl_2^-\cdot/Cl^-$ couple (2.0 V) should allow for the generation of chlorine radicals (eqs 4.4c and 4.5c), whose decay rate constants to Cl_2 are in the order of 10^9 M^{-1} s^{-1} .[7] Regardless of the terminal step in the mechanism, the RCS generation is

characterized as first order in [Cl^-] with a pseudo-steady-state approximation on $MO_x(ClO^-)$.[25] At circum-neutral pH, the Cl_2 reacts with water to form hypochlorous acid, hypochlorite, H^+, and Cl^- (eqs 4.5a and 4.5b).

$$MO_{x+1} + Cl^- \xrightarrow{k_{4a}} MO_x(ClO^-) \quad (4.4a)$$

$$MO_x(ClO^-) + Cl^- + 2H^+ \xrightarrow{k_{4b}} MO_x + Cl_2 + H_2O \quad (4.4b)$$

$$MO_x(ClO^-) + Cl^- + H^+ \longrightarrow MO_x(\cdot OH) + Cl_2^{-}\cdot \quad (4.4c)$$

$$Cl_2 + H_2O \xleftrightarrow[k_{-5a}]{k_{5a}} HOCl + Cl^- + H^+ \quad (4.5a)$$

$$HOCl \xleftrightarrow[k_{-5b}]{k_{5b}} ClO^- + H^+ \quad (4.5b)$$

$$Cl_2^{-}\cdot \longleftrightarrow Cl\cdot + Cl^- \quad (4.5c)$$

In the subsequent scan in NaCl solution (dashed line in Figure 4.2), there was a significant decrease in the current onset potential to 1.06 V. The earlier onset of the anodic current observed in the chloride solution could be ascribed to the formation of chlorate, which is a major by-product detected in the wastewater electrolysis (*vide infra*), along with the build-up of the RCS during the initial scan. The second onset potential did not explicitly coincide with the *E* values of ClO_3^-/Cl_2 (1.47 V at pH 0, 0.97 V at pH 7), ClO_3^-/HOCl (1.44 V at pH 0, 0.92 V at pH 7), and ClO_3^-/ClO^- (1.36 V at pH 0, 0.94 V at pH 7) couple. However, given the bulk solution near neutral pH, it is conceivable to assume that HOCl or ClO^- should be the primary reductants leading to chlorate production (eq 4.6).[40,41] The reaction scheme described herein neglects perchlorate

formation and direct oxidation of chloride to chlorate,[42] which are reported to occur in a very high anodic bias (in the order of 10^3 A m^{-2} in terms of J).[40,43]

$$2MO_{x+1} + ClO^- \xrightarrow{k_{6a}} 2MO_x + ClO_3^- \quad (4.6a)$$

$$2MO_{x+1} + HOCl \xrightarrow{k_{6b}} 2MO_x + ClO_3^- + H^+ \quad (4.6b)$$

4.3.3. Electrochemical Kinetics in Dilute Chloride Solutions. The polarization curve of Figure 4.1c shows an inflection in the current response with an augmentation of J in 30 and 50 mM NaCl solutions. An incremental transition of the Tafel slope is generally interpreted as an artifact of a mass transport limitation or a shift in the RDS[24]. If we consider that the RDS at a low E_a is due to the electron transfer reaction of eq 4.1, then the reactions involving the MO_{x+1} (eqs 4.3b, 4.4a, and 4.6) become important as the E_a increases. In the chemical reaction limited regime, heterogeneous reactions including OER, CER, and chlorate evolution reactions should not significantly depend on the $E_a - iR$.[23] At a relatively large value of η, the active sites would be virtually saturated with the higher oxide valence states; *i.e.*, quasi constant [MO_{x+1}] in the Nernstian equilibrium between MO_x and MO_{x+1}. If we define free chlorine (FC) as the sum of Cl_2, HOCl, and ClO^-,[14,28,40] then the electrochemical conversion of the chloride can be treated as a simple first-order reaction in series, where the overall kinetics is governed by eqs 4.7 – 4.9 (the complete derivation given in Supporting Information). Even in the presence of chlorine radicals, their short lifetimes should allow the [RCS] to be comparable with [FC], which was quantified as Cl_{DPD} in this study. The utilization of the FC as a single component can be rationalized by an existence of the most abundant reaction intermediate, whose

speciation would be dependent on the wastewater composition and the operating condition.

$$\frac{d[Cl^-]}{dt} = -k_{4a}[MO_{x+1}][Cl^-] = -k_4^{eff}[Cl^-] \quad (4.7)$$

$$\frac{d[FC]}{dt} = k_{4a}[MO_{x+1}][Cl^-] - k_{6a}[MO_{x+1}]^2[FC] = k_4^{eff}[Cl^-] - k_6^{eff}[FC] \quad (4.8)$$

$$\frac{d[ClO_3^-]}{dt} = k_{6a}[MO_{x+1}]^2[FC] = k_6^{eff}[FC] \quad (4.9)$$

Figure 4.4 shows the evolution of the Cl^-, FC, and ClO_3^- concentrations during a potentiostatic electrolysis in chloride solutions with initial chloride concentrations ($[Cl^-]_0$) of 30 and 50 mM. Anionic chlorine species with other oxidation states (ClO_2^-, ClO_4^-) were not detected. Despite the different current response (J = 232 ± 20 A m^{-2} in $[Cl^-]_0$ of 30 mM, 364 ± 23 A m^{-2} in 50 mM), the concentration of each chlorine species when normalized by $[Cl^-]_0$ is governed by identical kinetic parameters. This observation demonstrates that the CER and chlorate evolution reactions are in chemical reaction limited regime. The chlorate evolution rate was found to increase with time; this provides further corroboration that the oxidation of FC is responsible for the chlorate formation.[40,41] The apparent first-order behavior for the reactions taking place on the BiO_x/TiO_2 anode suggests that a plug-flow or sequential-batch reactor would be preferred to a continuous stirred-tank reactor in terms of the yield and selectivity for the FC. The least-squares estimates for the rate coefficients are 0.17 hr^{-1} for k_4^{eff} and 0.37 hr^{-1} for k_6^{eff} using all data sets. However, there are some deviations from the regression lines that are most likely due to potential interference of cathodic reactions, which reduce the RCS to

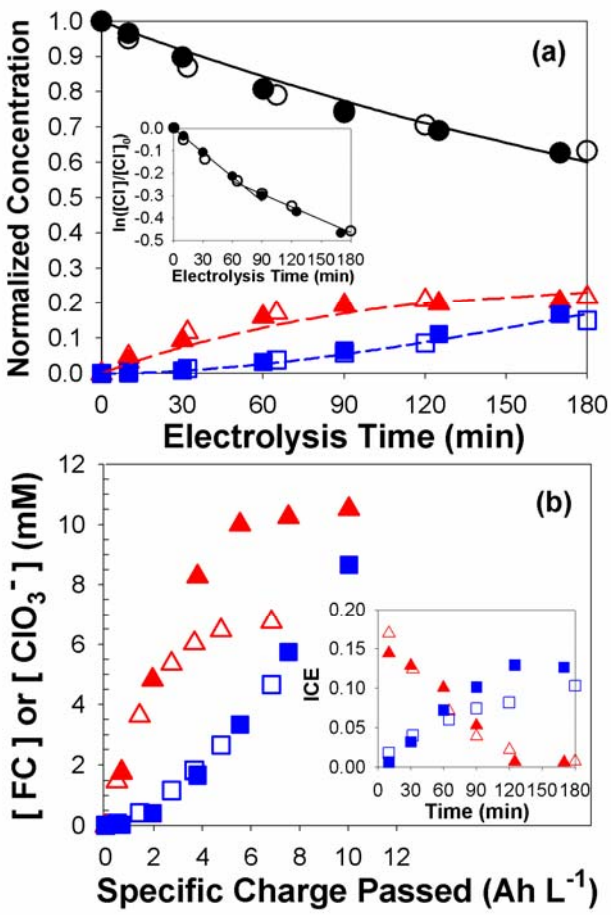

Figure 4.4. The variation of chloride (circle), free chlorine (triangle), and chlorate (square) concentration as a function of (a) electrolysis time and (b) specific charge passed during potentiostatic (E_a: 3 V) electrolysis in 30 mM (filled, R: 7.0 Ω) and 50 mM (empty, R: 5.0 Ω) NaCl solution (55 mL). The inset figures in (a) and (b) show the logarithmic normalized chloride concentration and the instantaneous current efficiency versus the electrolysis time.

chloride.[7,15] As shown in Figure 4.4a (inset), the k_4^{eff} slightly decreased with the augmentation of the FC concentration. The cathodic FC reduction constitutes a null electrochemical cycle with the Cl species as an electron relay,[7] reducing the apparent rate and current efficiency of the desired reactions (pollutants removal and hydrogen generation). With another least-squares estimation using the initial data points, we

obtained 0.24 hr^{-1} for k_4^{eff} and 0.36 hr^{-1} for k_6^{eff}, which can be used to estimate the rate constants for the homogeneous reactions between the RCS and electron donors (*vide infra*).

The instantaneous current efficiency (ICE) and general current efficiency (GCE) are figures of merit, which have been frequently used to evaluate the selectivity of the passed charge towards the chemical contaminants oxidation or RCS generation.[4,6] For an electrolysis cell with chloride and water as electron donors, the ICE for FC and chlorate can be expressed as follows (from eqs 4.3b, 4.8, and 4.9):

$$ICE_{FC} = \frac{i_{FC}}{i_{O_2} + i_{FC} + i_{ClO_3^-}} = \frac{2(k_4^{eff}[Cl^-] - k_6^{eff}[FC])}{2k_3^{eff} + 2k_4^{eff}[Cl^-] + 4k_6^{eff}[FC]} = \frac{2VFd[FC]}{i\,dt} \quad (4.10)$$

$$ICE_{ClO_3^-} = \frac{i_{ClO_3^-}}{i_{O_2} + i_{FC} + i_{ClO_3^-}} = \frac{4k_6^{eff}[FC]}{2k_3^{eff} + 2k_4^{eff}[Cl^-] + 4k_6^{eff}[FC]} = \frac{4VFd[ClO_3^-]}{i\,dt} \quad (4.11)$$

where, i_{O2}, i_{FC}, and i_{ClO3}- refer to the current used for generation of oxygen, FC, and chlorate, k_3^{eff} represents $k_{3b}[MO_{x+1}]$, while V is electrolyte volume and F is Faraday's constant. Figure 4.4b depicts [FC] and $[ClO_3^-]$ as a function of the specific charge passed for which the tangential slope is proportional to the ICE. The GCE at a specific time, defined as the charge required for an observed product divided by the total passed charge, is visualized by the slope of a secant line toward the initial point. As readily expected from eqs 4.10 and 4.11 and the analytical solutions of eqs 4.7 – 4.9 (eqs 4.34 and 4.36), the ICE_{FC} monotonically decreases along with the electrolysis time or passed charge, while the GCE_{FC} is always higher than the ICE_{FC} (*vice versa* for the chlorate). The initial ICE_{FC} should be a strong function of $[Cl^-]_0$ (eq 4.35), consistent with the literature on

chlorine evolution with metal oxide electrodes.[9,44] However, the initial ICE_{FC} was near 0.15 irrespective of the difference in $[Cl^-]_0$, while the effects of $[Cl^-]_0$ were more discernible for the initial ICE for chlorate formation. This observation indicates that the OER is not completely determined by the MO_{x+1} dismutation (eq 4.3b), but is also influenced by the electron transfer reactions (eqs 4.1 and 4.2), where k_3^{eff} could increase in part with the σ or $[Cl^-]_0$.

The observed first-order decrease of $[Cl^-]$ can also be a consequence of a mass transport limitation, whose impact can be roughly assessed by the limiting current density (J_L) as shown in eq 4.12:[34,45]

$$J_L = n\,F\,k_m^{\,Cl}\,[Cl^-], \tag{4.12}$$

where, n is the number of electrons for Cl^- oxidation (2) and k_m^{Cl} is the mass transfer coefficient for Cl^-. If k_m^{Cl} is assumed to be on the order of 10^{-5} m s^{-1},[46,47] then the J_L can be estimated to be 96 A m^{-2} for 50 mM NaCl solutions and 58 A m^{-2} for 30 mM solutions. These values are approximately 70% higher than the current density used for the FC formation (J multiplied by ICE_{FC}). This implies that chloride oxidation would not be in the transport-controlled regime. Even if a mass transport limitation is operative, the forms of kinetic equations are essentially the same.

4.3.4. Electrochemical Treatment of Fresh Urine. Preliminary experiments were performed to assess the performance of the WEC when fresh human urine is oxidized under potentiostatic condition (E_a: 3 V). During the electrochemical oxidation, intense foaming was observed, most likely due to an interaction of the electrolytically produced

bubbles (*i.e.*, O_2 and H_2) with proteins. In addition, precipitation of $CaCO_3$ and $Mg(OH)_2$ occurred on the cathode. The scale deposition is facilitated by high pH in the vicinity of the cathodes, presumably due to the consumption of protons during hydrogen production. In this situation, subsequent electrolyses were carried using fresh urine that was diluted with Milli-Q water by a volume ratio of 1:3. The cathodic deposit in calcareous form was corroborated by monotonic decreases of [Ca^{2+}] and [Mg^{2+}], as shown in Figure 4.5b (inset).

In spite of the $[Cl^-]_0$ in diluted urine of 45 mM, the observed rate of Cl^- decay as well as the production rates of FC and ClO_3^- (as shown in Figure 4.5a) were much smaller than those measured in NaCl solution. In this experiment, the Cl_{DPD} can be composed of either FC or combined chlorine, although each contribution cannot be estimated precisely by the chlorine mass balance analysis (see analytical details in the Supporting Information) due to the bulk pH (6.6) smaller than the pKa of HOCl (7.5). The slower kinetics that were observed during the chlorine redox cycle can be attributed to facile homogeneous reactions of FC, with the various electron donors present in urine being reduced back to chloride rather than further oxidized to chlorate. However, there was little net elimination of COD after 6 h (Figure 4.5b), which is most likely due to the presence of macro-molecular organic compounds. The proteins concentration in the diluted urine was 8 times higher than in the DWW (Table 4.1). The decomposition of high-molecular-weight organic compounds, which may be refractory to dichromate digestion in COD analysis, may have caused partial increase of the detectable COD. Since E of $Cr_2O_7^{2-}/Cr^{3+}$ (1.36 V at pH 0) exceeds the corresponding potentials of ClO^-/Cl^- or $HOCl/Cl^-$ at circum-neutral pH, the FC would transform the recalcitrant organics

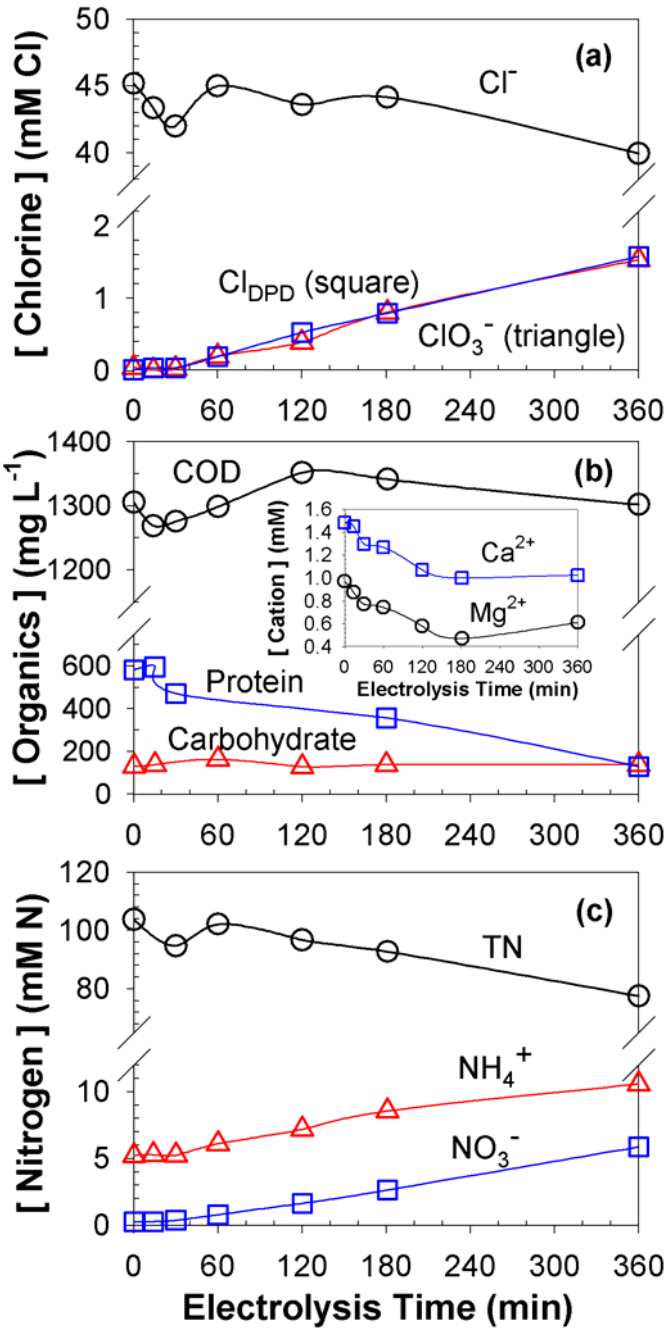

Figure 4.5. Evolution of (a) chlorine species, (b) organic species, (c) nitrogen species, and (b inlet) cations (Ca^{2+}, Mg^{2+}) concentration in a potentiostatic (E_a: 3 V) WEC experiment (J: 247 ± 6 A m^{-2}, $E_a - iR$: 2.15 ± 0.02 V, $E_a - E_c$: 5.41 ± 0.04 V) with diluted human urine (pH: 6.6, σ: 6.05 mS/cm, 55 mL).

to be kinetically amenable to the dichromate. The concentration profile of protein (Figure 4.5b), in terms of the abundance of peptide bonds determined via the Lowry method,[31] gave a pseudo first-order rate coefficient of 0.23 hr^{-1}; this indicates that the organic transformation by the FC involves cleavages of the peptide bonds.

About 80% of the initial TN in diluted urine was contributed by urea (Table 4.1) with additional contributions from creatinine, uric acid, amino acids, and protein. Figure 4.5c shows that the degradation of the nitrogen containing organics resulted in the production of ammonium ion, nitrate, and gaseous nitrogen expressed by the decrease in the TN concentration. The urea degradation by the FC is known to initiate by sequential chlorination of the urea to tetrachlorourea which is further oxidized to the chloramine species.[48] The inorganic combined chlorine eventually yields ammonium ion, nitrogen gas (by dismutation of chloramines in so-called breakpoint chlorination mechanism), and nitrate via further oxidation by FC.[9,49,50] The high concentration of refractory organics in the fresh urine required an extended electrolysis time for apparent COD conversion. In light of this observation, a combination with biological pre-treatment including anaerobic digestion is used to enhance pollutants conversion and to increase the energy efficiency of the electrochemical treatment,[34,36,47] as demonstrated in this study (*vide infra*).

4.3.5. Chlorine Transformation in the WEC with Model Septic Tank Effluents. During the potentiostatic (E_a: 3 V) WEC experiments with STEs, J was observed to be comparable to those in sodium chloride solution (Figure 4.6a). Therefore, we assume that the redox kinetics for the various chlorine species are in a chemical reaction limited regime. The main oxidizable components in the STEs were ammonium ion and organic

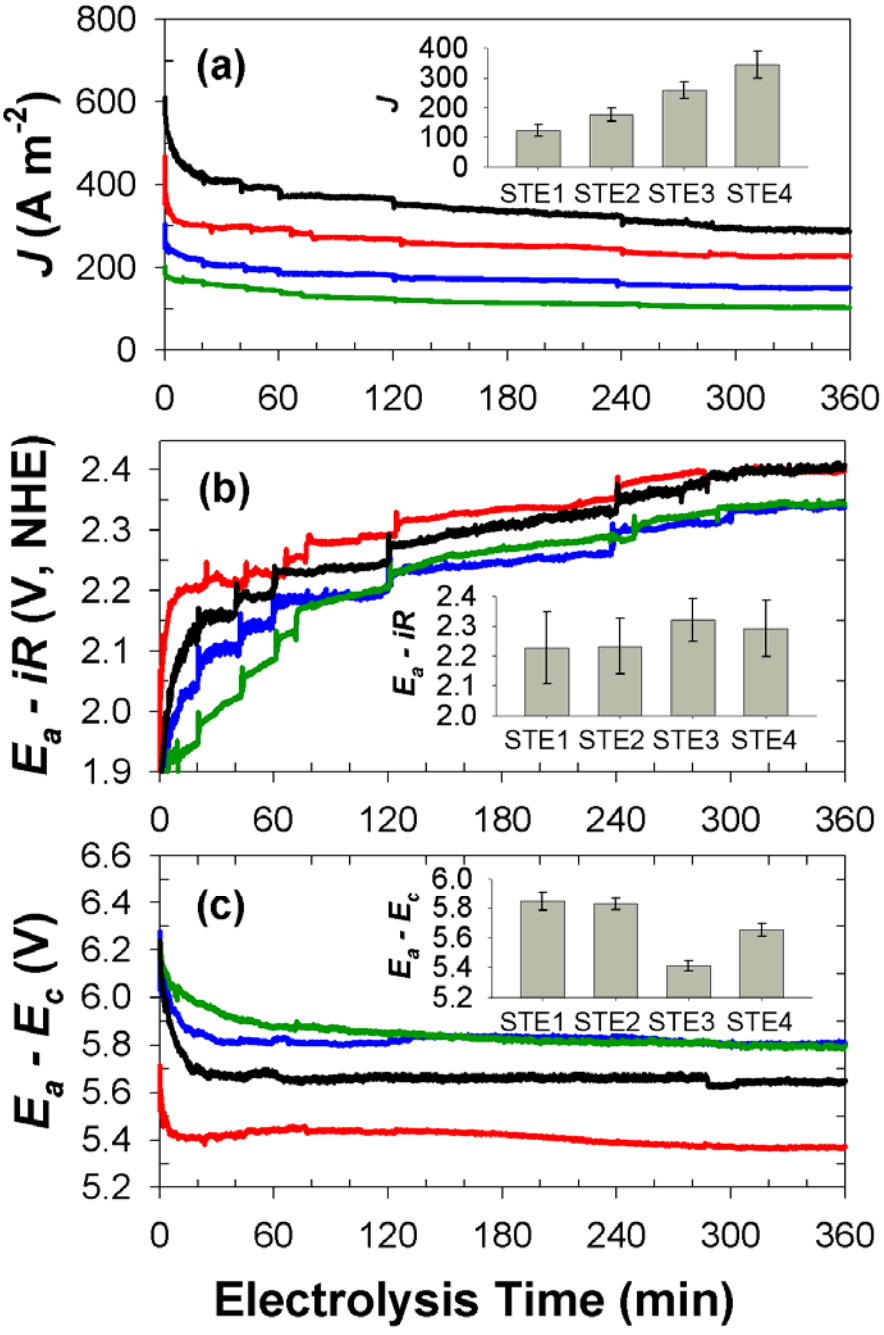

Figure 4.6. Evolution of (a) current density (J), (b) iR-compensated anodic potential ($E_a - iR$), and (c) cell voltage ($E_a - E_c$) in potentiostatic (E_a: 3 V) WEC experiment with model septic tank effluents; STE1 (green), STE2 (blue), STE3 (red), STE4 (black). Each inset figure shows the mean value with standard deviation in the error bars.

compounds in terms of COD (Table 4.1). Their homogeneous reactions with the FC can be expressed by the following non-stoichiometric reactions:

$$COD + FC \xrightarrow{k_{13}} Product + Cl^- \quad (4.13)$$

$$2NH_4^+ + 3FC \xrightarrow{k_{14}} N_2 + 3Cl^- \quad (4.14)$$

$$NH_4^+ + 4FC \xrightarrow{k_{15}} NO_3^- + 4Cl^- \quad (4.15)$$

Assuming that bimolecular reactions occur between the ammonium ion and FC with overall second order kinetics would be ideal, since reactions 14 and 15 are most likely to proceed via sequential chlorination, producing chloramines as reaction intermediates.[9] In this context, the governing equations for FC in the presence of oxidizable chemical species can be modified as:

$$\frac{d[FC]}{dt} = k_4^{eff}[Cl^-] - k_6^{eff}[FC] - k_{13}[FC][COD] - (3k_{14}+4k_{15})[FC]\left[NH_4^+\right] \quad (4.16)$$

Figure 4.7 illustrates the evolution of Cl_{DPD}, following a typical break-point chlorination curve,[49] whose concentration was much smaller than $[Cl^-]_0$. In addition, the sum of apparent $[Cl^-]$, including $[ClO^-]$, $[ClO_3^-]$ and $[Cl_{DPD}]$, was always conserved with standard deviations less than 0.1 mM. The initial pH of the STEs was near 9 (Table 4.1) due to urea hydrolysis during anaerobic pre-treatment. The bulk pH did not change significantly during electrolysis because of the inherent buffering capacity of STEs and bicarbonate generation from COD oxidation. Therefore, Cl_{DPD} should be dominated by the sum of the combined chlorines, which followed a typical time profile for intermediates of reactions in series. The insignificant concentrations of FC again imply

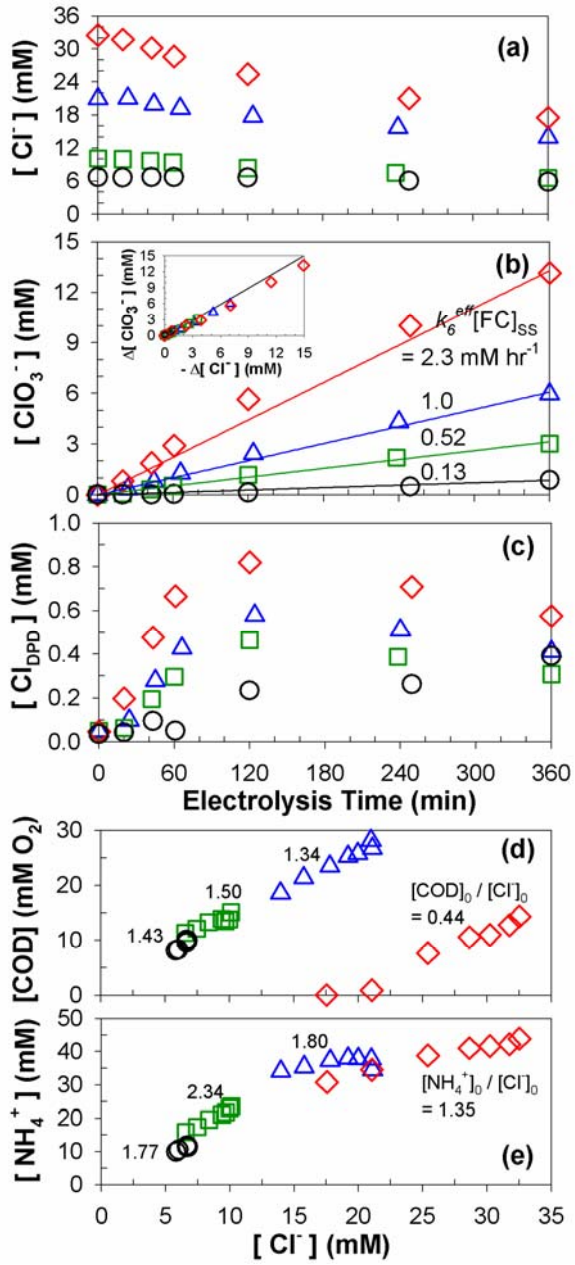

Figure 4.7. Time profiles of (a) chloride, (b) chlorate, and (c) Cl_{DPD} concentration together with (b, inset) scatter plots of increase of chlorate versus decrease of chloride concentration, (d) COD versus chloride concentration, and (e) ammonium ion versus chloride concentration in potentiostatic (E_a: 3 V) WEC experiments with model septic tank effluents; STE1 (circle), STE2 (square), STE3 (triangle), STE4 (diamond).

facile homogeneous reactions between FC and the constituent pollutants, which allows for a pseudo-steady-state approximation for the FC concentration ($[FC]_{SS}$). With a quasi-constant FC concentration, eq 4.16 indicates a linear correlation of $[Cl^-]$ with [COD] and $[NH_4^+]$ for each experimental condition, as demonstrated in Figure 4.7d and 4.7e. At given values of k_4^{eff} and k_6^{eff} under quasi-saturated active sites, the $[FC]_{SS}$ will be a function of the initial chloride concentration ($[Cl^-]_0$), the initial ratio of pollutants to chloride concentration ($[COD]_0/[Cl^-]_0$, $[NH_4^+]_0/[Cl^-]_0$), and the rate coefficients for specific pollutant degradation (k_{13}, k_{14}, k_{15}).

In the STEs electrolysis, a major by-product was again found to be chlorate ion, whose production rate appeared to be nearly unchanged with time (zero-order kinetics), as shown in Figure 4.7b and expressed by eq 4.9 at a constant $[FC]_{SS}$. Using the value of k_6^{eff}, the $[FC]_{SS}$ recorded in the slopes of the chlorate concentration profiles were estimated to be 0.34, 1.4, 2.8 and 6.3 mM (higher than the bulk $[Cl_{DPD}]$). As noted in the literature,[34] there should be concentration gradients for the heterogeneous reactants and products in electrode vicinity, often referred to boundary layer or reaction cage. Owing to higher reactivity and molecular weight, the FC gradient would be more pronounced than the chloride gradient so that the $[FC]_{SS}$ in the boundary layer can exceed the bulk $[FC]_{SS}$. Given our previous arguments, the characteristic mass balance equations can be written for the near-surface of the anode and bulk solution separately as:

$$\frac{d[FC]^A_{SS}}{dt} = k_4^{eff}[Cl^-] - k_6^{eff}[FC]^A_{SS} - \frac{k_m^{FC}}{\delta}\left([FC]^A_{SS} - [FC]^B_{SS}\right) = 0 \quad (4.17)$$

$$\frac{d[FC]^B_{SS}}{dt} = \frac{k_m^{FC}}{\delta}\left([FC]^A_{SS} - [FC]^B_{SS}\right) - [FC]^B_{SS}\left\{k_{13}[COD] + (3k_{14} + 4k_{15})\left[NH_4^+\right]\right\} = 0 \quad (4.18)$$

In this case, $[FC]^{A}_{SS}$ and $[FC]^{B}_{SS}$ are the quasi-steady-state FC concentrations in the boundary layer and in bulk, k_m^{FC} is the mass transfer coefficient for the FC, and δ is the depth of boundary layer. When $[FC]^{B}_{SS}$ is much lower than $[FC]^{A}_{SS}$ and the k_m^{FC}/δ is constant, eqs 4.17 and 4.43 indicate that $[FC]^{A}_{SS}$ and the corresponding chlorate production rate are strongly dependent on the initial chloride concentration,[40] as shown in Figure 4.7b. On the other hand, as can be inferred from eq 4.18, $[FC]^{B}_{SS}$ should be affected by the initial concentration of pollutants ($[COD]_0$, $[NH_4^+]_0$) as well.

4.3.6. COD Removal Characteristics in WEC with Model Septic Tank Effluents. Figure 4.8 illustrates the evolution of the COD concentration during the WEC experiments using STEs. The COD conversion after 6 h electrolysis was 15%, 25%, and 34% for STE1–3, whereas almost complete mineralization (*i.e.*, conversion to CO_2) of COD was observed for STE4. The pseudo-steady-state assumption for FC allows us to characterize the COD degradation kinetics by a pseudo-first-order rate constant, k_{COD}^{eff}.

$$\frac{d[\mathrm{COD}]}{dt} = -k_{13}[\mathrm{FC}]^{\mathrm{B}}_{\mathrm{SS}}[\mathrm{COD}] = -k_{COD}^{eff}[\mathrm{COD}] \qquad (4.19)$$

From a series of nonlinear regressions of eq 4.19 we can estimate k_{COD}^{eff}, which is an order of magnitude higher for STE4 (0.43 hr^{-1}) than for the others (0.041 – 0.066 hr^{-1}). The rate constants depend on $[COD]_0/[Cl^-]_0$ rather than $[Cl^-]_0$, in agreement with previous reports[14,33,51] in which the observed rate constants increased with the relative COD concentration but were not altered by influent dilution. The initial ratio of pollutants-to-chloride concentration would be an important determinant of $[FC]^{B}_{SS}$, as inferred from eq 4.18 with $[FC]^{A}_{SS}$ as a strong function of $[Cl^-]_0$. Therefore, an extended

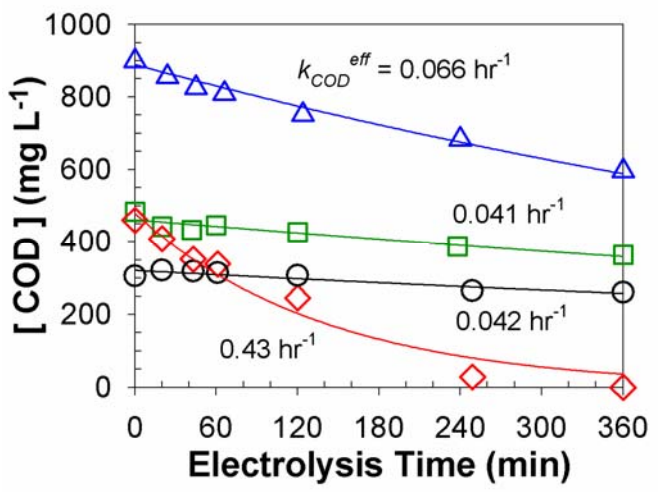

Figure 4.8. Time profiles of COD concentration in potentiostatic (E_a: 3 V) WEC experiments with model septic tank effluents; STE1 (circle), STE2 (square), STE3 (triangle), STE4 (diamond).

anaerobic treatment resulted in STE4 having a lower pollutants-to-chloride ratio than the other STEs (Figure 4.7d and 4.7e) and superior COD conversion. In addition, a lower fraction of recalcitrant organics in STE4 (Table 4.1) also contributed to the higher k_{COD}^{eff} by an augmented k_{13}. Assuming the DWW is analogous to the flushing water for excreta, the recipe of STE4 is rationalized by a low usage of flushing water, which is threefold volume of urine, as would be the scenario in communities with water shortages. The HRT required for STE with a higher flushing would be comparable since the dilution does not affect the ratio of pollutants to chloride concentration, or even smaller when sticking to an effluent water quality criteria.

Consequently, the results for STE4 strongly demonstrate that our WEC is suitable for efficient toilet wastewater treatment system in a relatively short HRT without external chemical dosages, if combined with proper anaerobic pre-treatment unit. It should be

noted that the pre-treatment would require much shorter times than 7 days, since the biological concentration in septic tanks would be much greater than in DWW.

Figure 4.9 details the transformation characteristics for the organic compounds in terms of scatter plots for protein, carbohydrates, and carboxylic acids versus the COD concentration. As in the case of COD, the pseudo first-order rate constant for protein degradation ($k_{protein}^{eff}$) was also much higher for STE4 (2.5 hr^{-1}) than for STE1–3 (1.2 – 1.5 hr^{-1}). In addition, the observed $k_{protein}^{eff}$ exceeds k_{COD}^{eff} by more than an order of magnitude for STE1–3, which suggests that the FC would preferentially attack the nucleophilic sites of organic macromolecules by electrophilic substitution reactions.[7,52] The reactions between FC and the peptides, which have second-order rate constants on the order of $10^6 – 10^7$ $M^{-1}s^{-1}$, are known to initiate by chloramination of terminal amine group.[52] The cleavage of peptides bonds should produce measurable COD (carbonyl compounds and amines with shorter chain lengths), because initial protein degradation was not accompanied by a noticeable decrease of COD (Figure 4.9a). On the contrary, the COD degradation caused increases in carbohydrate and carboxylate concentration (Figure 4.9b and 4.9c), as is reported in a previous work using municipal wastewater.[19] While carboxylate ions (*e.g.*, formate, oxalate, and acetate) are often the observed products of organic compound oxidation,[39,53] the increase in apparent carbohydrate may be due to the release of mono- or oligo-saccharide from decompositions of glycoproteins. The reaction of FC with electron-rich glycosidic bonds in poly-saccharides should also yield simple sugars, which can form hydroxymethylfurfural in the phenol/sulphuric acid analytical method.[32] The reactivity of the FC with oxygenated moieties (alcohol and carboxyl functional groups) in carbohydrates and carboxylic acids are known to be

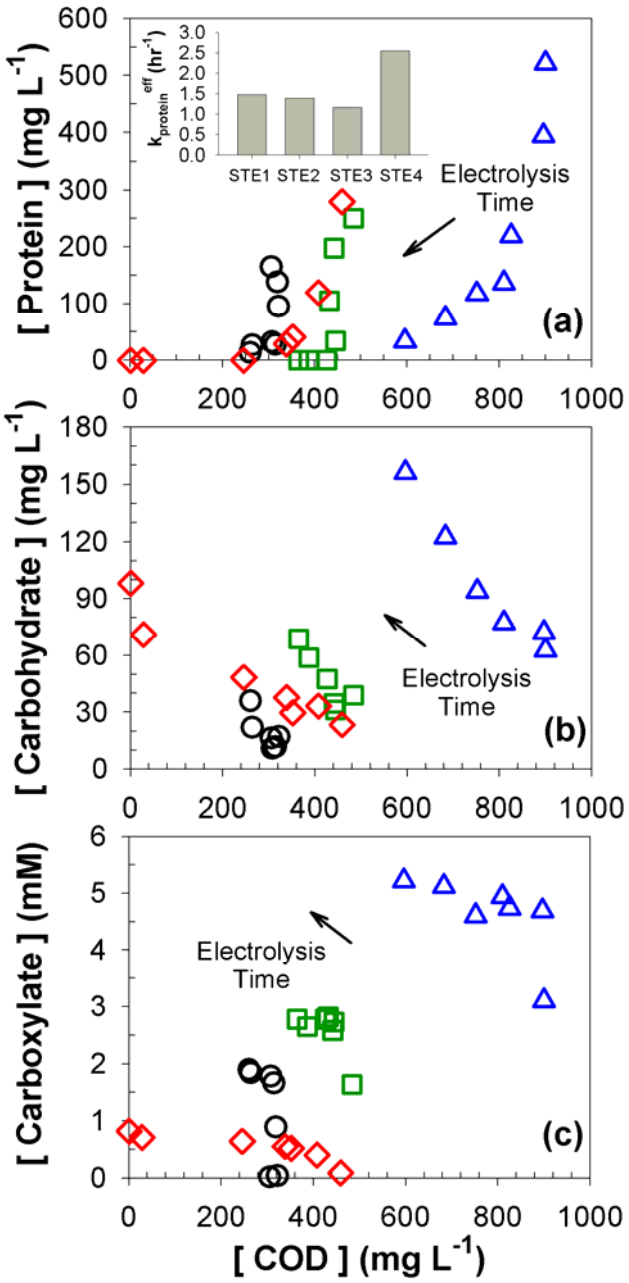

Figure 4.9. Scatter plot for (a) protein, (b) carbohydrate, and (c) carboxylates concentration versus COD concentration together with (a, inlet) pseudo-first-order rate constants for protein degradation in potentiostatic (E_a: 3 V) WEC experiments with model septic tank effluents; STE1 (circle), STE2 (square), STE3 (triangle), STE4 (diamond). Arrows indicate an arbitrary varying direction along with time.

relatively slow.[52,54] Nevertheless, the accumulation of these organic compounds did not significantly contribute to the residual COD of STE4.

4.3.7. Nitrogen Removal Characteristics in the WEC with Model Septic Tank Effluents. The evolution of nitrogen containing compounds, another major constituent of STEs, is illustrated in Figure 4.10. The conversions of TN and NH_4^+ after the 6 h of electrolysis were observed to be less than that of COD, and the TN conversion had a relative order of STE4 (39%) > STE2 (25%) > STE3 (18%) > STE1 (13%). The kinetics of the ammonium ion oxidation can be described in terms of the pseudo-first-order rate constants, k_{am}^{eff}, as follows:

$$\frac{d[NH_4^+]}{dt} = -(3k_{14}+4k_{15})[FC]^B_{SS}[NH_4^+] = -k_{am}^{eff}[NH_4^+] \quad (4.20)$$

As shown in Figure 4.10b, the magnitude of k_{am}^{eff} was not simply correlated with $[FC]^B_{SS}$ as in the case of COD, and the highest rate constant was observed for STE2. Table 4.1 and Figure 4.10a (inset) show that ammonium ion constituted 60 – 70% of TN in STE3–4 and even larger fractions for STE1–2 (higher dilution with DWW). The initial organic nitrogen, in terms of $[TN]_0 - [NH_4^+]_0 - [NO_3^-]_0$, was attributed to urea by more than 50%. As discussed above, the degradation of urea and other nitrogen containing moieties (amines, amides, amino acids, and peptides) will produce ammonium ion via organic chloramine formation and consecutive oxidation.[48,52] As a result, apparent k_{am}^{eff} values were lower for STE3–4 despite the higher levels of $[FC]^B_{SS}$. Figure 4.10a (inset) further visualizes that the ostensible decay rates of TN exceeds those of ammonium for STE3–4. This observation together with low values of $[Cl_{DPD}]$ (Figure 4.7c) suggests that

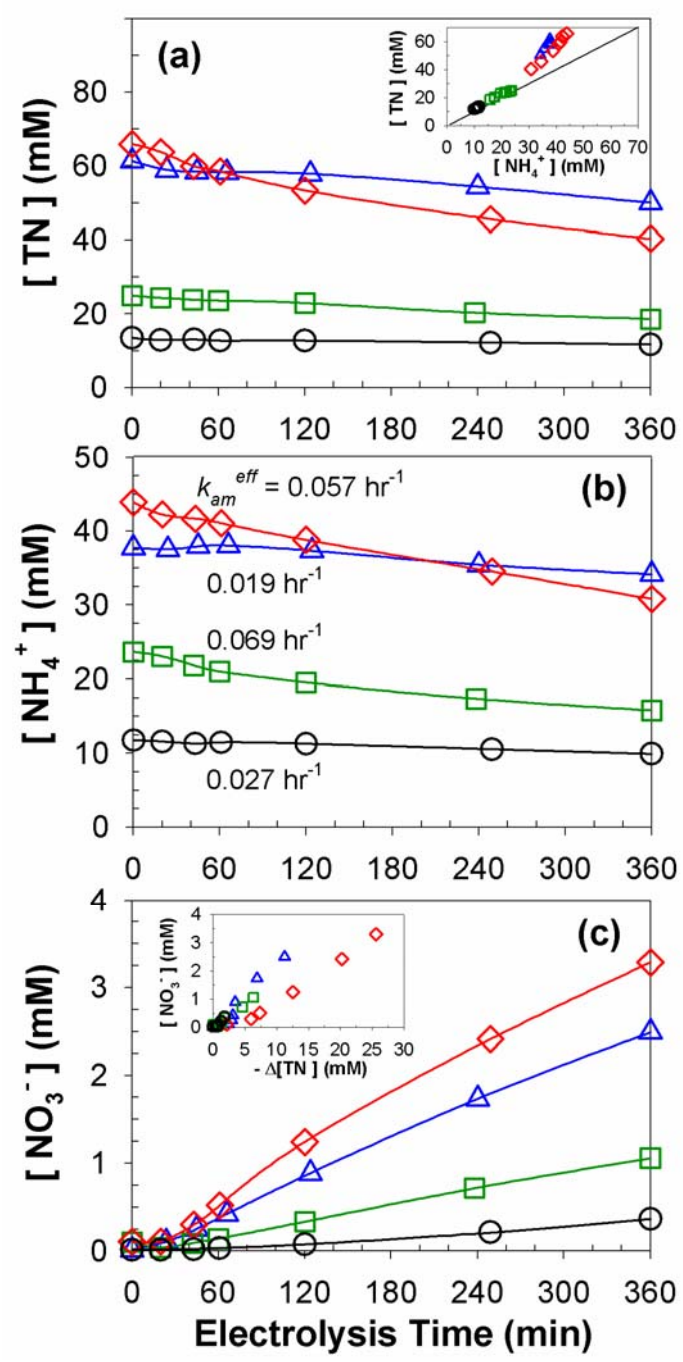

Figure 4.10. Time profiles of (a) TN, (b) NH_4^+, and (c) NO_3^- concentration together with scatter plots for (a, inlet) TN versus NH_4^+ concentration and (c, inlet) NO_3^- versus removed NH_4^+ concentration in potentiostatic (E_a: 3 V) WEC experiments with model septic tank effluents; STE1 (circle), STE2 (square), STE3 (triangle), STE4 (diamond).

gaseous nitrogen generation may not be limited by the dismutation reactions of the chloramine species. The relative reactivity of FC towards amides (including urea) is not as high as the second-order rate constants of FC with ammonium ion, primary/secondary amines, amino acids, and peptides.[52] On the other hand, the observed rates of the TN decay were also greater than nitrate generation rate, as shown in Figure 4.10c (inset), which is more obvious for STE4. Although the mechanism and kinetics for the breakpoint chlorination are not fully known, the dominance of combined chlorine in the Cl_{DPD} allows us to conclude that the disproportionation of chloramines is favored relative to their further oxidation to nitrate, as the chloramine concentration increases. Previous studies on ammonium ion removal from landfill leachates[50] and anaerobic digestion effluents[55] reported similar results in that N_2 formation is favored over nitrate formation as J or $[Cl^-]_0$ increase.

In the case of the STE4 effluent, which had the highest TN conversion, the WEC effluents still had significant nitrogen concentrations (~ 40 mM TN), which were primarily in the form of ammonium ion (76%) and nitrate (8.2%). If we imagine the bioavailability of residual nitrogen, the treated water can then be regarded as a liquid fertilizer if used for irrigation water.

4.3.8. Current Efficiency and Energy Consumption of the WEC with Model Septic Tank Effluents. Based on the kinetic model in this study, the instantaneous current efficiencies for COD degradation and for production of N_2, NO_3^-, and ClO_3^- can be expressed as follows:

$$ICE_{COD} = \frac{4k_{14}[FC]^{B}_{SS}[COD]}{2k_3^{eff} + 2k_4^{eff}[Cl^-] + 4k_6^{eff}[FC]^{A}_{SS}} = -\frac{4VFd[COD]}{i\,dt} \quad (4.21)$$

$$ICE_{N_2} = \frac{3k_{14}[FC]^{B}_{SS}[NH_4^+]}{2k_3^{eff} + 2k_4^{eff}[Cl^-] + 4k_6^{eff}[FC]^{A}_{SS}} = -\frac{3VFd[TN]}{i\,dt} \quad (4.22)$$

$$ICE_{NO_3^-} = \frac{8k_{15}[FC]^{B}_{SS}[NH_4^+]}{2k_3^{eff} + 2k_4^{eff}[Cl^-] + 4k_6^{eff}[FC]^{A}_{SS}} = \frac{8VFd[NO_3^-]}{i\,dt} \quad (4.23)$$

$$ICE_{ClO_3^-} = \frac{6k_6^{eff}[FC]^{A}_{SS}}{2k_3^{eff} + 2k_4^{eff}[Cl^-] + 4k_6^{eff}[FC]^{A}_{SS}} = \frac{6VFd[ClO_3^-]}{i\,dt} \quad (4.24)$$

In these equations, the [COD] should be expressed in molar concentration units (mM O_2), while N_2 is assumed to totally account for the gaseous nitrogen production. The ICE for chlorate production is expressed based on 6-electron transferred from chloride. Compared to the ICE for chloride oxidation in the absence of pollutants (eqs. 4.10 – 4.11, Figure 4.4b) with significant time variations, the differential concentrations of COD, TN, nitrate, and chlorate appeared to be almost linearly correlated with the specific charge passed (Figure 4.11). Accordingly, the ICE did not deviate much from the GCE. These findings can be explained in terms of the pseudo first-order rate constants for pollutant degradation (k_{COD}^{eff}, kam^{eff}) that are much lower than k_4^{eff} and k_6^{eff}. The ICE for organic compound degradation on non-active electrodes such as BDD has sometimes been reported to approach unity initially but decrease with time, as limited by the mass transport of substrate to the anode surface.[54]

A series of linear regressions of the differential concentrations on the specific charge passed can be used to estimate the mean current efficiencies, as illustrated by Figure 4.12a. The results as well as eqs 4.44 – 4.47 indicate that the current efficiencies of the

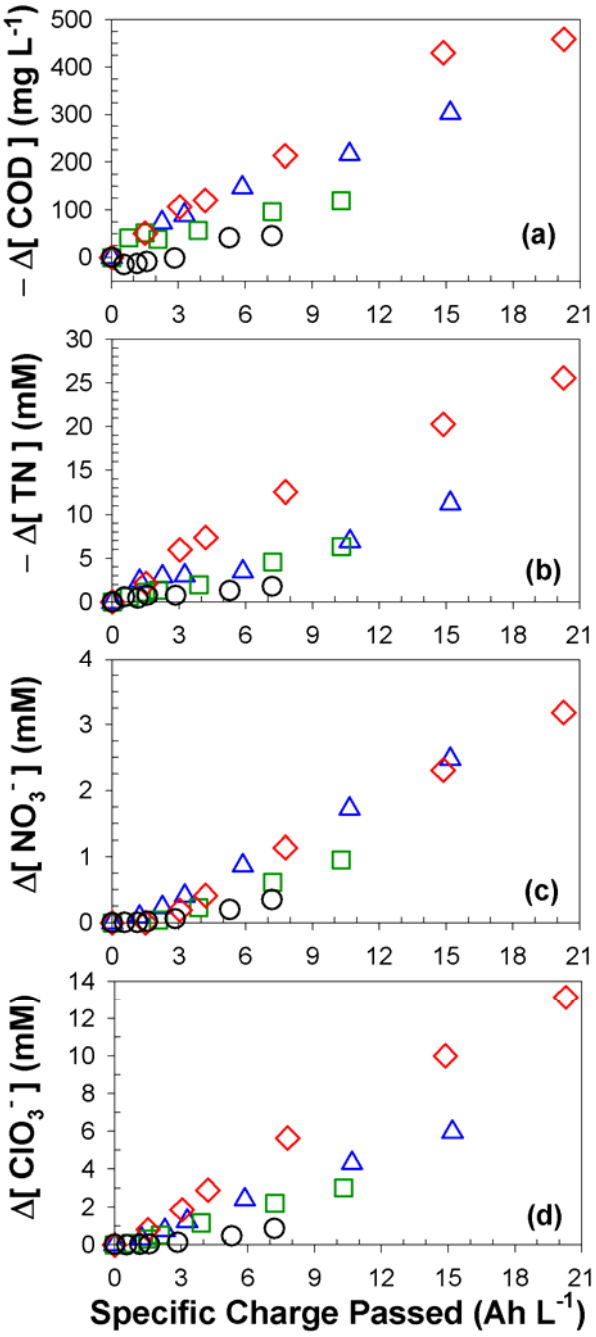

Figure 4.11. Variations in (a) COD concentration, (b) TN concentration, (c) nitrate concentration, and (d) chlorate concentration as a function of specific passed charge in potentiostatic (E_a: 3 V) WEC experiments with model septic tank effluents; STE1 (circle), STE2 (square), STE3 (triangle), STE4 (diamond).

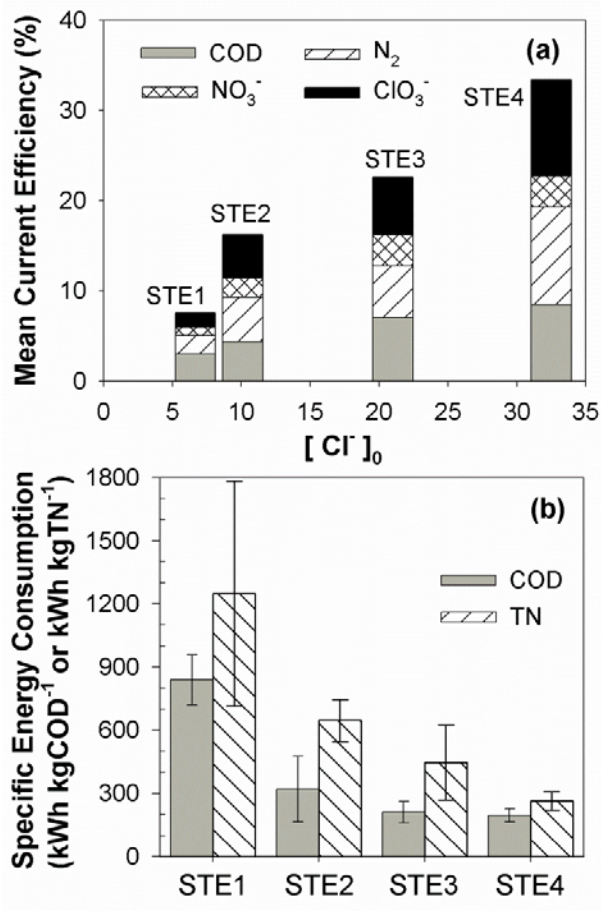

Figure 4.12. (a) Average current efficiency for COD, nitrogen, and chlorine conversion, and (b) specific energy consumption for COD and total nitrogen on average in potentiostatic (E_a: 3 V) WEC experiments with model septic tank effluents. Error bars represent the standard deviation.

FC mediated oxidation are influenced substantially by $[Cl^-]_0$ itself,[10,13,28,56] rather than by the pollutants-to-chloride ratio. The rate of pollutant removal should be a function of $[Cl^-]_0$ only, since it is proportional to the $[FC]^B_{SS}$ multiplied by the pollutant concentrations. At a given $[Cl^-]_0$, eqs. 4.44 – 4.47 further indicate that the relative concentration and reactivity towards the FC govern the charge consumption for each substrate. For example, in STE4, k_{COD}^{eff} exceeds k_{am}^{eff} by a greater extent than in the other STEs, which was

balanced by the lowest value of the [COD]/[NH_4^+] ratio. Independent of the specific STE composition, the charge required for COD reduction was comparable with that for N_2 production, about half of which was consumed for nitrate production. Even though the 'regression toward the mean' analysis would underestimate the individual ICE, the sum of eqs 4.21 to 4.24 as the total current used other than OER was less than 50%. In a previous direct measurement of oxygen evolution from an electrolysis of a chloride solution, we estimated the current efficiency of the OER to be less than 25%.[15]

As can be seen in Figure 4.12b, the energy consumption for unit removal of pollutants also monotonically decreased with the increase in $[Cl^-]_0$. However, the influence of $[Cl^-]_0$ on the SEC is not as significant as on the ICE due to the large increment of J with $[Cl^-]_0$ (Figure 4.6a). These observations suggest that an influent dilution (increase in flushing volume) might reduce the HRT to achieve an effluent quality criteria (*vide supra*), but an increase of energy consumption is inevitable.[14,51] The kinetic model presented herein predicts minor effects of J on the observed rate constants in the chemical reaction limited regime. This model is in general agreement with previous reports on RuO_2 which experimentally showed a saturation dependence of the observed rate constants on J.[12,33,34,57] It is clear that current density plays a crucial role in the direct oxidation rate but not in the indirect oxidation rate.[33,57] Under these conditions, further increases in J should favor OER rather than CER, which in turn decreases the current efficiency of pollutant oxidation but significantly increases the solution resistance, energy loss and SEC.[14] Therefore, a reduction in SEC is expected with an effort to adjust the E_a to maximize the desired current efficiency.

4.3.9. Hydrogen Production in WEC with Model Septic Tank Effluents. Figure 4.13 depicts the quantitative estimates for hydrogen generation as a function of the average J value. The rate of total gas production (Q) almost linearly increased with the average J. The volumetric fraction of hydrogen (X_{H2}) was about 40% under current densities less than 150 A m^{-2} (STE1), while increased to near 60% at higher current densities. However, the dependency of X_{H2} on J was not obvious when taking into account the measurement error (coefficient of variation: 11% in maximum) in the GC/TCD analysis. The adverse contribution of gases initially present in the connection tube may explain the lower X_{H2} for STE1. The remaining fractions of the gaseous products would include oxygen, water vapor, nitrogen, carbon dioxide, chlorine, ammonia, and hydrogen sulphide (with minor contribution). The molar flow rate of hydrogen (F_{H2}) is used to estimate the current efficiency for hydrogen generation (CE_{H2}) to be 50% for STE1, increasing to 90% for STE2–4. The hydrogen evolution reaction (HER) has a well-known reaction sequence[20] that proceeds by combination of eq 4.25 with either eq 4.26 or 4.27:

$$HA + C + e^- \rightarrow C(H\cdot) + A^- \quad (4.25)$$

$$C(H\cdot) + HA + e^- \rightarrow H_2 + C + A^- \quad (4.26)$$

$$2\,C(H\cdot) \rightarrow H_2 + 2C \quad (4.27)$$

where C stands for a cathodically active site for the HER and A is the conjugate base of the proton (OH^- or null term in circum-neutral pH). The main constituent acting as the active sites is presumed to be Ni, in the case of Hastelloy C-22 that was used in this study. Ni belongs to a near-summit group of the volcano plots under basic conditions.[20]

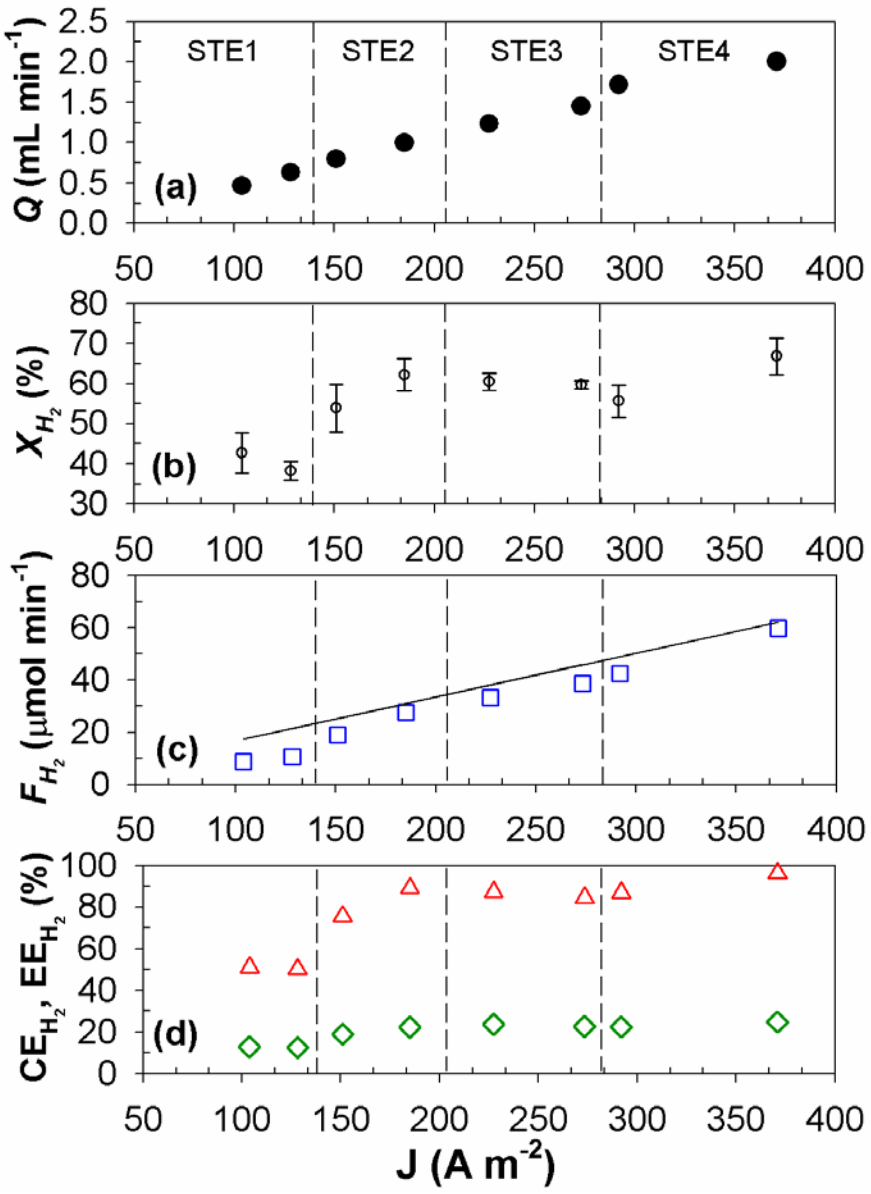

Figure 4.13. Dependency of (a) generation rate of total gaseous products (Q, solid circle), (b) volumetric fraction of hydrogen (X_{H2}, void circle), (c) molar generation rate of hydrogen (F_{H2}, square), (d) current and energy efficiency (CE in triangle and EE in diamond) for hydrogen generation on average current density (J) during gas collection (80 – 110 min and 300 – 330 min) in potentiostatic (E_a: 3 V) WEC experiments with model septic tank effluents. Error bars in (b) represent the standard deviations of repetitive GC/TCD measurement, and the reference line in (c) shows theoretical F_{H2} with CE of 100%.

Ni-based binary or ternary metal composites (with Mo, Co, Cd, and Fe) have been thoroughly investigated for their catalytic HER activity that is dependent on the bond strength between the metal surface and adsorbed hydrogen.

Competitive electron acceptors including oxygen, nitrate, chlorate, and FC can interfere with the HER. The cathodic potential (E_c), which ranged from –2.4 to –2.8 V, is sufficiently below the E of $O_2/HO_2\cdot$ (–0.54 V at pH 7) as well as positive E (spontaneous reduction) of NO_3^-/NO_2^- (0.42 V at pH 7), ClO_3^-/ ClO^-, and ClO^-/Cl^-. The RCS species are clearly the major scavengers of HER and their effects on the CE_{H2} have been documented in our previous reports. For example, Park *et al.*[7] reported that an injection of organic electron donors during electrolysis in NaCl solution results in a sharp increase of CE_{H2} by quenching the RCS. In the present report, anodically generated FC species should engage in facile reactions with pollutants in the bulk phase before being transported to the cathode surface,[34] as demonstrated by the quasi-steady-state FC with a very small bulk-phase concentration ($[FC]^B_{SS}$). The reduction of oxygen to superoxide radical and resulting reactive oxygen species (ROS) were thought to influence the oxidation of pollutants. However, the roles of ROS appear to be marginal in this study because the conversion of COD was insignificant when the chloride concentration was low (STE1).

In spite of the relatively high current efficiency, the energy efficiency for hydrogen generation (EE_{H2}) was observed near 25% for STE2–4, which is much lower than an idealized electrolysis unit. The EE_{H2} has been reported to increase with lowering cell voltage[19] and in synergy with photocatalytic hydrogen evolution on the BiO_x/TiO_2

electrode under direct solar radiation.[18] The energy losses due to the intrinsic overpotential, the ohmic drop, along with the various side reactions in the complex electrolyte system within the WEC may be compensated by a net saving of energy for water treatment and the added costs of electrolyte addition. The US DOE[58] estimated that the wastewater collection and treatment consumes about 60% of the energy requirements for water supply. The impurities in the gaseous product narrow the usage of the hydrogen to an internal combustion (IC) engine without an added purification procedure. Based on the energy efficiency of the current hydrogen IC engines of 35%, a 10% reduction of the SEC is expected with using the hydrogen as a secondary energy source for the WEC.

4.4. OUTLOOK FOR THE FUTURE

Conventional water reuse criteria for non-restricted urban reuse applications are generally based on a BOD of 30 mg L^{-1}.[3] The electrochemically treated water for the STE4 showed negligible COD, suggesting that the treated water is suitable for reuse as toilet flushing water and for irrigation. The relatively facile removal of protein further implies an efficient disinfection of coliforms through complete breakage of bacterial cells and inactivation owing to the reduced carbon source. Since color is also an important consideration for reuse of treated wastewater, we note that the yellowish color was nearly eliminated during WEC treatment as shown in Figure 4.14. However, chlorate production poses a potential health risk, since several drinking water guidelines recommend chlorate concentrations lower than 10 μM.[40] The high level of chlorate most likely will not be a significant problem when using the treated water only for toilet flushing. The chlorate

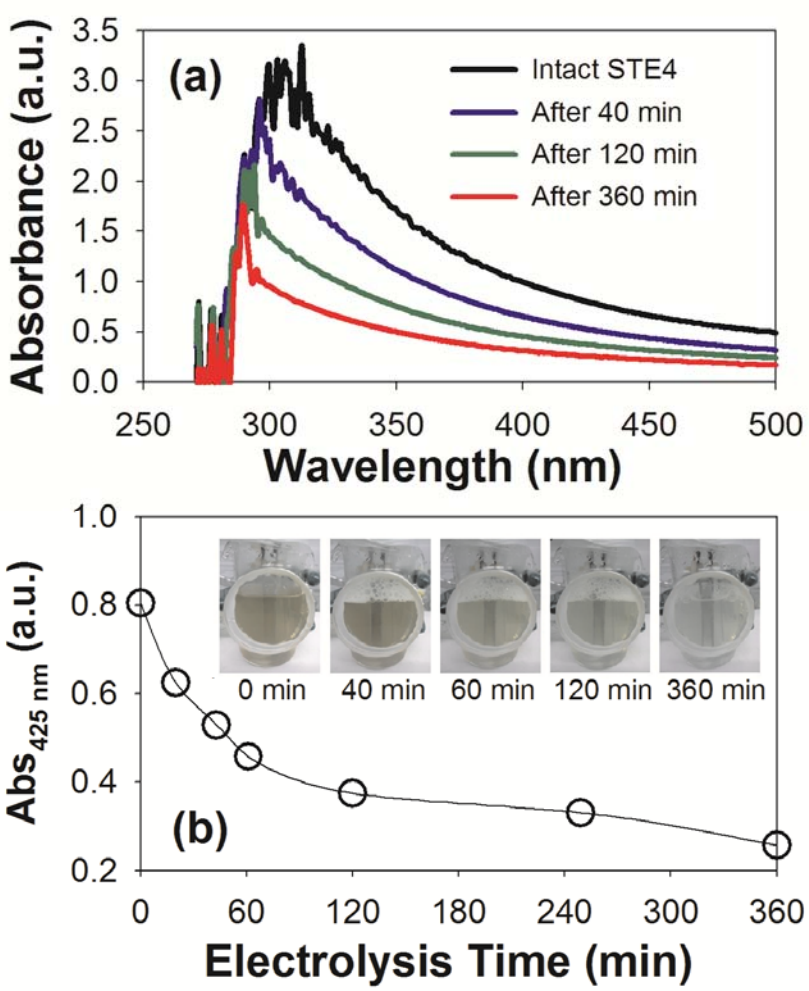

Figure 4.14. (a) Variation in absorbance spectra (270 – 500 nm) along with the electrolysis time and (b) absorbance at 425 nm as a function of electrolysis time in potentiostatic (E_a: 3 V) WEC experiments with STE4. Inset figure in (b) visualizes the color variation.

formation can be reduced with an increase in hydraulic mixing in the WEC resulting in an increase of k_m^{FC}, as inferred from eqs 4.40 and 4.43. A proper selection of cathode materials, known to have a high activity for nitrate reduction (such as bimetallic Cu/Zn[59]), can be another potential solution to facilitate chlorate reduction to chloride under actual operating conditions. These enhancements would be beneficial with respect to increasing

the efficiency of pollutant oxidation even though chlorate reduction could compete with the HER. Calcareous deposits on the cathode surface could result in significant mass transport limitation for hydrogen evolution. Current switching (*i.e.*, polarity) has been shown to remove calcareous deposits, although this would require anti-corrosion cathode material.

The WEC with or without a PV power source has the potential to meet the growing demand for on-site wastewater treatment coupled with water reuse and, in select cases, for alternative fuel production from water-splitting. A scaled-up WEC or PWEC should be easy to transport to various environments, including urbanized areas, peri-urban environments, and remote locations in the developing world that lack viable sanitation facilities to treat domestic black water. These systems may also be used for treatment of industrial wastewaters, landfill leachates, anaerobic sludge digester effluents, and reverse osmosis concentrates.

4.5. SUPPORTING INFORMATION

4.5.1. Materials. NaCl and concentrated sulfuric acid were used as received from Macron Chemicals. Crystalline phenol (99.6%) and $Na_2C_2O_4$ were purchased from J.T. Baker. Total Protein Reagent, Folin-Ciocalteu's phenol reagent, protein standard (bovin serum albumin), $TiOSO_4$, H_2IrCl_6, $[O_2CCH_2C(OH)(CO_2)CH_2CO_2]Bi$, Bi_2O_3, $SnCl_4$, and $TaCl_5$ were received from Sigma Aldrich. Chemical oxygen demand (COD) digestion solution, COD standard solution (potassium acid phthalate), total nitrogen (TN) reagent set, DPD total chlorine reagent powder, and chlorine standard solution were received from Hach. Jack Bean Urease was provided by the Worthington Biochemical Corporation. All other

chemicals were supplied by Mallinckrodt. Ti metal sheet (Ti-Gr.2 sheet, 0.50 mm thick) was purchased from ThyssenKrupp Materials. All electrolyte and standard solutions were prepared in MilliQ water (18.2 MO cm) from a Millipore Milli-Q gradient water purification system.

4.5.2. BiO_x/TiO_2 Electrode Preparation. A Ti metal sheet (0.5 mm thick) was sand-blasted with SiC paper (120 – 240 grits) and degreased with acetone. The precursor solution for the anti-passivation layer was prepared as 73 mM H_2IrCl_6 with 27 mM $TaCl_5$ in 4 M HCl solution. Both sides of pretreated Ti support were brushed by the precursor and annealed at 525 °C for an hour. This procedure was repeated 5 times with the same annealing temperature for a 10 min duration. A sealing coat was deposited twice by painting 225 mM $SnCl_4$ and 12.5 mM Bi_2O_3 in 0.5 M HCl solution and baking at 425 °C for 10 min. Precipitates from dissolving 10 mmol Bi_2O_3 and 0.48 mol $TiOSO_4$ in 1.2 M Na_2CO_3 (1 L) were calcined at 830 °C for 45 min to produce bismuth oxide doped titanium dioxide (BiO_x/TiO_2) nanoparticles. The precursor for the BiO_x/TiO_2 thin film (overcoat solution) was 160 mM $Ti(OCH_2CH_2O)_2$ (*i.e.*, the preparation details are described elsewhere) with 80 mM $[O_2CCH_2C(OH)(CO_2)CH_2CO_2]Bi$ in a 0.24 M NH_4OH solution. To prepare the slurry deposition layer, BiO_x/TiO_2 particles dispersed in MilliQ water (3 M metal concentration) were brushed on air dried; after this step a 25-fold diluted overcoat solution was sequentially pasted on to the surface. The slurry deposit was baked on at 250 for 5 min; this procedure was repeated 7 times. In the final sequence, a thin film of BiO_x/TiO_2 deposit was made by repetitive sealing with overcoat solution annealed at 250 °C (4 times) and then at 450 °C (2 times).

4.5.3. Electrochemical Methods. Before all electrochemical experiments, the electrodes were rinsed with acetone and a large amount of MilliQ water. The electrode module was allowed to equilibrate with the electrolyte solution in an open circuit for 1 h while monitoring the open circuit potential of anode and cathode. As a routine procedure, the pH, conductivity, and the ohmic resistance between anode and reference electrode (R) were measured before and after the electrochemical experiments. The R was measured by current interruption method with current bias of 100 mA. For the chrono-voltammetric data collection, the current intensity (J) was averaged from 400 to 500 seconds. The variation of current density after 500 seconds was not significant, since the p-values of the paired t-test between the averaged current from 400 to 500 seconds and from 500 to 1800 seconds were always larger than 0.05.

4.5.4. Model Septic Tank Effluent Preparation. The COD degradation during the anaerobic incubation followed an exponential decay trend, where initial decomposition of macro-molecules was followed by mineralization of organics with exponential growth of microorganisms, initially presented in domestic wastewater (DWW). Urea was hydrolyzed to give ammonium ion enzymatically using urease; this resulted in an increase of the pH of the model septic tank effluents (STEs) up to 9. The increase in pH resulted in a considerable amount of precipitation of minerals, including magnesium ammonium phosphate (struvite). The supernatant of the collected DWW and prepared STEs was used in the experiments to minimize the effects of particulate matters.

4.5.5. Analyses. COD was measured with standard digestion kits with a low detection range (3 – 150 mg L^{-1}); the kits were prepared in order to eliminate the interference of the ammonium ion in the COD analysis[60] by controlling the kinetics for ammonium and COD

oxidation steps separately. Samples were diluted to adjust the chloride concentration far below the interference range (2,000 mg L^{-1}) as suggested by the digestion kit supplier (Hach, USA). For the Dionex DX-500 Ion Chromatography (IC) system, hypochlorite appeared to have a peak at a retention time identical to the chloride ion with superimposable calibration curves. Since the hypochlorite would be detected both in the IC analysis and total chlorine (Cl_{DPD}) analysis, the sum of [Cl^-], [Cl_{DPD}], and [ClO_3^-] exceeded the initial chloride concentration, particularly for the electrolysis in pure NaCl solution. In this case, [Cl^-] was calibrated by subtracting the difference, which corresponds to [ClO^-]. For urea measurement, 5 mL of diluted samples in 15 mL conical tubes were added by 2 mL of urease solution (63.1 mg L^{-1}) and incubated in water bath (50 °C) for 20 min. Treated samples were cooled down at room temperature (RT) for IC analysis. Urea measurements were performed only for the intact electrolyte before the electrolysis due to the interference of free chlorine. In the phenol-sulfuric acid method,[32] 0.4 mL samples in glass tubes were mixed with 0.4 mL phenol solution (5 W/V%) and 2 mL sulfuric acids (95%) to measure the absorbance at 470 nm after reaction for 30 min at RT. For protein measurement,[31] 0.5 mL samples were introduced to 2.5 mL total protein reagent in 15 mL conical tubes with gentle inversion several times. After reaction for 10 min at RT, twofold diluted Folin-Ciocalteu's phenol reagent of 0.2 mL was added with vigorous mixing. With further holding at RT for 30 min, the absorbance of the supernatant was measured at 600 nm. NH_4Cl, NaOCl, $NaClO_3$, $NaNO_2$, $NaNO_3$, HCOONa, $Na_2C_2O_4$, CH_3COONa, $MgSO_4$, and $CaCl_2$ were used as standards with proper concentration range for the IC analysis. Potassium acid phthalate, NH_4Cl, chlorine, bovine serum albumin, and glucose solution

were used as a standard for COD, TN, Cl_{DPD}, protein, and carbohydrate analysis, respectively.

4.5.6. Kinetic Equations in the Absence of Oxidizable Pollutants. eq 4.28 implies a pseudo-steady-state assumption for the surface bound ClO^-, while eq 4.30 is based on the negligible amount of Cl_2 at circum-neutral pH.

$$\frac{d[MO_x(ClO^-)]}{dt} = k_{4a}[MO_{x+1}][Cl^-] - k_{4b}[MO_x(ClO^-)][Cl^-][H^+]^2 = 0 \quad (4.28)$$

$$\frac{d[Cl^-]}{dt} = -k_{4a}[MO_{x+1}][Cl^-] - k_{4b}[MO_x(ClO^-)][Cl^-][H^+]^2 + k_{5a}[Cl_2] - k_{-5a}[HOCl][Cl^-][H^+] \quad (4.29)$$

$$\frac{d[Cl_2]}{dt} = k_{4a}[MO_{x+1}][Cl^-] - k_{5a}[Cl_2] + k_{-5a}[HOCl][Cl^-][H^+] = 0 \quad (4.30)$$

$$\frac{d[HOCl]}{dt} = k_{5a}[Cl_2] + k_{-5a}[HOCl][Cl^-][H^+] - k_{5b}[HOCl] + k_{-5b}[ClO^-][H^+] - k_{6b}[MO_{x+1}]^2[HOCl] \quad (4.31)$$

$$\frac{d[ClO^-]}{dt} = k_{5b}[HOCl] - k_{-5b}[ClO^-][H^+] - k_{6a}[MO_{x+1}]^2[ClO^-] \quad (4.32)$$

$$\frac{d[ClO_3^-]}{dt} = k_{6a}[MO_{x+1}]^2[ClO^-] + k_{6b}[MO_{x+1}]^2[HOCl] \quad (4.33)$$

Assuming that active sites are saturated at high current densities (quasi-constant $[MO_{x+1}]$), we use eq 4.28 and eq 4.30 in eq 4.29 to obtain

$$\frac{d[Cl^-]}{dt} = -k_{4a}[MO_{x+1}][Cl^-] = -k_4^{eff}[Cl^-] \quad (4.7)$$

By denoting $[FC] = [Cl_2] + [HOCl] + [ClO^-]$, eq 4.30 to 4.32 gives

$$\frac{d[FC]}{dt} = k_{4a}[MO_{x+1}][Cl^-] - k_{6a}[MO_{x+1}]^2[FC] = k_4^{eff}[Cl^-] - k_6^{eff}[FC] \quad (4.8)$$

Assuming that k_{6a} is comparable to k_{6b} and [FC] ~ [HOCl] + [ClO^-] at circum-neutral pH,

$$\frac{d[ClO_3^-]}{dt} = k_{6a}[MO_{x+1}]^2[FC] = k_6^{eff}[FC] \quad (4.9)$$

4.5.7. Instantaneous Current Efficiency (ICE) for Free Chlorine (FC) and Chlorate without the Presence of Pollutants. Substituting the analytical solutions of eq 4.7 to 4.9 to eq 4.10 yields,

$$ICE_{FC} = \frac{2[k_4^{eff}\exp(-k_4^{eff}t) - \frac{k_4^{eff}k_6^{eff}}{k_6^{eff} - k_4^{eff}}\{\exp(-k_4^{eff}t) - \exp(-k_6^{eff}t)\}]}{\frac{2k_3^{eff}}{[Cl^-]_0} + 2k_4^{eff}\exp(-k_4^{eff}t) + \frac{4k_4^{eff}k_6^{eff}}{k_6^{eff} - k_4^{eff}}\{\exp(-k_4^{eff}t) - \exp(-k_6^{eff}t)\}} \quad (4.34)$$

where, $[Cl^-]_0$ denotes the initial chloride concentration.

$$\text{When } t \to 0,\ ICE_{FC} = \frac{k_4^{eff}}{\frac{k_3^{eff}}{[Cl^-]_0} + k_4^{eff}} \quad (4.35)$$

Similarly, the instantaneous current efficiency for chlorate formation is expressed as

$$ICE_{ClO_3^-} = \frac{\frac{6k_4^{eff}k_6^{eff}}{k_6^{eff} - k_4^{eff}}\{\exp(-k_4^{eff}t) - \exp(-k_6^{eff}t)\}}{\frac{2k_3^{eff}}{[Cl^-]_0} + 2k_4^{eff}\exp(-k_4^{eff}t) + \frac{4k_4^{eff}k_6^{eff}}{k_6^{eff} - k_4^{eff}}\{\exp(-k_4^{eff}t) - \exp(-k_6^{eff}t)\}} \quad (4.36)$$

4.5.8. Kinetic Equations in the Presence of Pollutants. The governing equations for chloride and FC with the presence of pollutants are derived by modifying eq 4.7 and 4.8 as:

$$\frac{d[Cl^-]}{dt} = -k_4^{eff}[Cl^-] + k_{13}[FC][COD] + (3k_{14} + 4k_{15})[FC][NH_4^+] \quad (4.37)$$

$$\frac{d[FC]}{dt} = k_4^{eff}[Cl^-] - k_6^{eff}[FC] - k_{13}[FC][COD] - (3k_{14} + 4k_{15})[FC][NH_4^+] \quad (4.16)$$

By treating the FC mass balance analyses for the bulk-phase and the electrode boundary layer separately, we employ pseudo-steady-state approximations for the FC to give

$$\frac{d[\mathrm{FC}]^{\mathrm{A}}{}_{\mathrm{SS}}}{dt} = k_4^{eff}\left[\mathrm{Cl}^-\right] - k_6^{eff}[\mathrm{FC}]^{\mathrm{A}}{}_{\mathrm{SS}} - \frac{k_m^{FC}}{\delta}\left([\mathrm{FC}]^{\mathrm{A}}{}_{\mathrm{SS}} - [\mathrm{FC}]^{\mathrm{B}}{}_{\mathrm{SS}}\right) = 0 \tag{4.38}$$

$$\frac{d[\mathrm{FC}]^{\mathrm{B}}{}_{\mathrm{SS}}}{dt} = \frac{k_m^{FC}}{\delta}\left([\mathrm{FC}]^{\mathrm{A}}{}_{\mathrm{SS}} - [\mathrm{FC}]^{\mathrm{B}}{}_{\mathrm{SS}}\right) - [\mathrm{FC}]^{\mathrm{B}}{}_{\mathrm{SS}}\left\{k_{13}[\mathrm{COD}] + (3k_{14} + 4k_{15})[\mathrm{NH_4^+}]\right\} = 0 \tag{4.39}$$

where, $[\mathrm{FC}]^{\mathrm{A}}{}_{\mathrm{SS}}$ and $[\mathrm{FC}]^{\mathrm{B}}{}_{\mathrm{SS}}$ are quasi-steady-state FC concentration in the anode vicinity and in bulk, k_m^{FC} is the mass transfer coefficient for the FC, and δ is the depth of boundary layer. Since $[\mathrm{FC}]^{\mathrm{A}}{}_{\mathrm{SS}} >> [\mathrm{FC}]^{\mathrm{B}}{}_{\mathrm{SS}}$, the solutions of eq 4.38 and 4.39 are reduced to

$$[\mathrm{FC}]^{\mathrm{A}}{}_{\mathrm{SS}} = \frac{k_4^{eff}[\mathrm{Cl}^-]}{k_6^{eff} + k_m^{FC}/\delta} \equiv C_{[FC]^A{}_{SS}}[\mathrm{Cl}^-] \tag{4.40}$$

$$[\mathrm{FC}]^{\mathrm{B}}{}_{\mathrm{SS}} = \frac{\left(k_m^{FC}/\delta\right)k_4^{eff}[\mathrm{Cl}^-]}{\left(k_6^{eff} + k_m^{FC}/\delta\right)\left(k_{13}[\mathrm{COD}] + (3k_{14} + 4k_{15})[\mathrm{NH_4^+}]\right)} \equiv \frac{C_{[FC]^B{}_{SS}}[\mathrm{Cl}^-]}{\left(k_{13}[\mathrm{COD}] + (3k_{14} + 4k_{15})[\mathrm{NH_4^+}]\right)} \tag{4.41}$$

Also, the mass balance equation for chloride (eq 4.37) and chlorate (eq 4.9) are modified as

$$\frac{d[\mathrm{Cl}^-]}{dt} = -k_4^{eff}[\mathrm{Cl}^-] + k_{13}[\mathrm{FC}]^{\mathrm{B}}{}_{\mathrm{SS}}[\mathrm{COD}] + (3k_{14} + 4k_{15})[\mathrm{FC}]^{\mathrm{B}}{}_{\mathrm{SS}}\left[\mathrm{NH_4^+}\right] \tag{4.42}$$

$$\frac{d[\mathrm{ClO_3^-}]}{dt} = k_6^{eff}[\mathrm{FC}]^{\mathrm{A}}{}_{\mathrm{SS}} \tag{4.43}$$

4.5.9. Instantaneous Current Efficiency (ICE) for COD degradation. Substituting eq 4.40 and 4.41 into eqs 4.21 to 4.24 gives

$$\mathrm{ICE_{COD}} = \frac{4C_{[FC]^B{}_{SS}}}{\left(\frac{2k_3^{eff}}{[\mathrm{Cl}^-]} + 2k_4^{eff} + 4C_{[FC]^A{}_{SS}}k_6^{eff}\right)\left(1 + \frac{(3k_{14} + 4k_{15})[\mathrm{NH_4^+}]}{k_{13}[\mathrm{COD}]}\right)} \tag{4.44}$$

$$\mathrm{ICE_{N_2}} = \frac{4C_{[FC]^B{}_{SS}}}{\left(\frac{2k_3^{eff}}{[\mathrm{Cl}^-]} + 2k_4^{eff} + 4C_{[FC]^A{}_{SS}}k_6^{eff}\right)\left(1 + \frac{4k_{15}}{3k_{14}} + \frac{k_{13}[\mathrm{COD}]}{3k_{14}[\mathrm{NH_4^+}]}\right)} \tag{4.45}$$

$$ICE_{NO_3^-} = \frac{4C_{[FC]^B{}_{SS}}}{\left(\frac{2k_3^{eff}}{[Cl^-]} + 2k_4^{eff} + 4C_{[FC]^A{}_{SS}} k_6^{eff}\right)\left(1 + \frac{3k_{14}}{4k_{15}} + \frac{k_{13}[COD]}{4k_{15}[NH_4^+]}\right)} \quad (4.46)$$

$$ICE_{ClO_3^-} = \frac{6C_{[FC]^A{}_{SS}} k_6^{eff}}{\frac{2k_3^{eff}}{[Cl^-]} + 2k_4^{eff} + 4C_{[FC]^A{}_{SS}} k_6^{eff}} \quad (4.47)$$

4.6. REFERENCES

(1) Vorosmarty, C. J.; McIntyre, P. B.; Gessner, M. O.; Dudgeon, D.; Prusevich, A.; Green, P.; Glidden, S.; Bunn, S. E.; Sullivan, C. A.; Liermann, C. R.; Davies, P. M. Global threats to human water security and river biodiversity. *Nature* **2010,** *467* (7315), 555-561.

(2) Grant, S. B.; Saphores, J. D.; Feldman, D. L.; Hamilton, A. J.; Fletcher, T. D.; Cook, P. L. M.; Stewardson, M.; Sanders, B. F.; Levin, L. A.; Ambrose, R. F.; Deletic, A.; Brown, R.; Jiang, S. C.; Rosso, D.; Cooper, W. J.; Marusic, I. Taking the "Waste" out of "Wastewater" for human water security and ecosystem sustainability. *Science* **2012,** *337* (6095), 681-686.

(3) *Guidelines for water reuse*; EPA/600/R-12/618; United States Environmental Protection Agency: Washington, D.C., 2012.; nepis.epa.gov/Adobe/PDF/P100FS7K.pdf.

(4) Martinez-Huitle, C. A.; Ferro, S. Electrochemical oxidation of organic pollutants for the wastewater treatment: direct and indirect processes. *Chemical Society Reviews* **2006,** *35* (12), 1324-1340.

(5) Trasatti, S. Electrocatalysis in the anodic evolution of oxygen and chlorine. *Electrochimica Acta* **1984,** *29* (11), 1503-1512.

(6) Panizza, M.; Cerisola, G. Direct and mediated anodic oxidation of organic pollutants. *Chemical Reviews* **2009,** *109* (12), 6541-6569.

(7) Park, H.; Vecitis, C. D.; Hoffmann, M. R. Electrochemical water splitting coupled with organic compound oxidation: The role of active chlorine species. *Journal of Physical Chemistry C* **2009,** *113* (18), 7935-7945.

(8) Malpass, G. R. P.; Miwa, D. W.; Mortari, D. A.; Machado, S. A. S.; Motheo, A. J. Decolorisation of real textile waste using electrochemical techniques: Effect of the chloride concentration. *Water Research* **2007,** *41* (13), 2969-2977.

(9) Chiang, L. C.; Chang, J. E.; Wen, T. C. Indirect oxidation effect in electrochemical oxidation treatment of landfill leachate. *Water Research* **1995,** *29* (2), 671-678.

(10) Costa, C. R.; Olivi, P. Effect of chloride concentration on the electrochemical treatment of a synthetic tannery wastewater. *Electrochimica Acta* **2009,** *54* (7), 2046-2052.

(11) Malpass, G. R. P.; Miwa, D. W.; Machado, S. A. S.; Olivi, P.; Motheo, A. J. Oxidation of the pesticide atrazine at $DSA^{(R)}$ electrodes. *Journal of Hazardous Materials* **2006,** *137* (1), 565-572.

(12) Miwa, D. W.; Malpass, G. R. P.; Machado, S. A. S.; Motheo, A. J. Electrochemical degradation of carbaryl on oxide electrodes. *Water Research* **2006,** *40* (17), 3281-3289.

(13) Rajkumar, D.; Palanivelu, K. Electrochemical degradation of cresols for wastewater treatment. *Industrial & Engineering Chemistry Research* **2003,** *42* (9), 1833-1839.

(14) Rajkumar, D.; Kim, J. G. Oxidation of various reactive dyes with in situ electro-generated active chlorine for textile dyeing industry wastewater treatment. *Journal of Hazardous Materials* **2006,** *136* (2), 203-212.

(15) Park, H.; Vecitis, C. D.; Hoffmann, M. R. Solar-powered electrochemical oxidation of organic compounds coupled with the cathodic production of molecular hydrogen. *Journal of Physical Chemistry A* **2008,** *112* (33), 7616-7626.

(16) Choi, J.; Qu, Y.; Hoffmann, M. R. SnO_2, IrO_2, Ta_2O_5, Bi_2O_3, and TiO_2 nanoparticle anodes: electrochemical oxidation coupled with the cathodic reduction of water to yield molecular H_2. *Journal of Nanoparticle Research* **2012,** *14* (8).

(17) Valero, D.; Ortiz, J. M.; Exposito, E.; Montiel, V.; Aldaz, A. Electrochemical wastewater treatment directly powered by photovoltaic panels: Electrooxidation of a dye-containing wastewater. *Environmental Science & Technology* **2010,** *44* (13), 5182-5187.

(18) Park, H.; Bak, A.; Ahn, Y. Y.; Choi, J.; Hoffmannn, M. R. Photoelectrochemical performance of multi-layered BiO_x-TiO_2/Ti electrodes for degradation of phenol and production of molecular hydrogen in water. *Journal of Hazardous Materials* **2012,** *211*, 47-54.

(19) Park, H.; Choo, K.; Park, H.; Choi, J.; Hoffmann, M. R. Electrochemical oxidation and microfiltration of municipal wastewater with simultaneous hydrogen production: Influence of organic and particulate matter. *Chemical Engineering Journal* **2013,** *215-216* (15), 802-810.

(20) Walter, M. G.; Warren, E. L.; McKone, J. R.; Boettcher, S. W.; Mi, Q. X.; Santori, E. A.; Lewis, N. S. Solar water splitting cells. *Chemical Reviews* **2010,** *110* (11), 6446-6473.

(21) Panizza, M.; Cerisola, G. Electrochemical oxidation as a final treatment of synthetic tannery wastewater. *Environmental Science & Technology* **2004,** *38* (20), 5470-5475.

(22) Panizza, M.; Delucchi, M.; Cerisola, G. Electrochemical degradation of anionic surfactants. *Journal of Applied Electrochemistry* **2005,** *35* (4), 357-361.

(23) Comninellis, C. Electrocatalysis in the electrochemical conversion/combustion of organic pollutants for waste-water treatment. *Electrochimica Acta* **1994,** *39* (11-12), 1857-1862.

(24) Trasatti, S. Progress in the understanding of the mechanism of chlorine evolution at oxide electrodes. *Electrochimica Acta* **1987,** *32* (3), 369-382.

(25) Krishtalik, L. I. Kinetics and mechanism of anodic chlorine and oxygen rvolution reactions on yransition-metal oxide electrodes. *Electrochim Acta* **1981**, *26* (3), 329-337.

(26) Gujar, T. P.; Shinde, V. R.; Lokhande, C. D.; Han, S. H. Electrosynthesis of Bi_2O_3 thin films and their use in electrochemical supercapacitors. *Journal of Power Sources* **2006,** *161* (2), 1479-1485.

(27) Shuk, P.; Wiemhofer, H. D.; Guth, U.; Gopel, W.; Greenblatt, M. Oxide ion conducting solid electrolytes based on Bi_2O_3. *Solid State Ionics* **1996,** *89* (3-4), 179-196.

(28) Scialdone, O.; Randazzo, S.; Galia, A.; Silvestri, G. Electrochemical oxidation of organics in water: Role of operative parameters in the absence and in the presence of NaCl. *Water Research* **2009,** *43* (8), 2260-2272.

(29) Weres, O. Electrode with surface comprising oxides of titanium and bismuth and water purification process using this electrode. U.S. Patent 7,494,583 B2, Feb. 24, 2009.

(30) *Onsite wastewater treatment systems manual*; EPA/625/R-00/008; United States Environmental Protection Agency: Washington, D.C., 2002.; nepis.epa.gov/Adobe/ PDF/P100FS7K.pdf .

(31) Lowry, O. H.; Rosebrough, N. J.; Farr, A. L.; Randall, R. J. Protein measurement with the Folin phenol reagent. *Journal of Biological Chemistry* **1951,** *193* (1), 265-275.

(32) Dubois, M.; Gilles, K. A.; Hamilton, J. K.; Rebers, P. A.; Smith, F. Colorimetric method for determination of sugars and related substances. *Analytical Chemistry* **1956,** *28* (3), 350-356.

(33) Mohan, N.; Balasubramanian, N. In situ electrocatalytic oxidation of acid violet 12 dye effluent. *Journal of Hazardous Materials* **2006,** *136* (2), 239-243.

(34) Szpyrkowicz, L.; Kelsall, G. H.; Kaul, S. N.; De Favei, M. Performance of electrochemical reactor for treatment of tannery wastewaters. *Chemical Engineering Science* **2001,** *56* (4), 1579-1586.

(35) Wang, Y.; Wang, Y.; Meng, Y. L.; Ding, H. M.; Shan, Y. K.; Zhao, X.; Tang, X. Z. A highly efficient visible-light-activated photocatalyst based on bismuth- and sulfur-codoped TiO_2. *Journal of Physical Chemistry C* **2008,** *112* (17), 6620-6626.

(36) Goncalves, M. R.; Marques, I. P.; Correia, J. P. Electrochemical mineralization of anaerobically digested olive mill wastewater. *Water Research* **2012,** *46* (13), 4217-4225.

(37) Kesselman, J. M.; Weres, O.; Lewis, N. S.; Hoffmann, M. R. Electrochemical production of hydroxyl radical at polycrystalline Nb-doped TiO_2 electrodes and estimation of the partitioning between hydroxyl radical and direct Hole oxidation pathways. *Journal of Physical Chemistry B* **1997,** *101* (14), 2637-2643.

(38) Santana, M. H. P.; De Faria, L. A. Oxygen and chlorine evolution on RuO_2+TiO_2+CeO_2+Nb_2O_5 mixed oxide electrodes. *Electrochimica Acta* **2006,** *51* (17), 3578-3585.

(39) Panizza, M.; Cerisola, G. Olive mill wastewater treatment by anodic oxidation with parallel plate electrodes. *Water Research* **2006,** *40* (6), 1179-1184.

(40) Jung, Y. J.; Baek, K. W.; Oh, B. S.; Kang, J. W. An investigation of the formation of chlorate and perchlorate during electrolysis using Pt/Ti electrodes: The effects of pH and reactive oxygen species and the results of kinetic studies. *Water Research* **2010,** *44* (18), 5345-5355.

(41) Polcaro, A. M.; Vacca, A.; Mascia, M.; Palmas, S.; Ruiz, J. R. Electrochemical treatment of waters with BDD anodes: kinetics of the reactions involving chlorides. *Journal of Applied Electrochemistry* **2009,** *39* (11), 2083-2092.

(42) Czarnetzki, L. R.; Janssen, L. J. J. Formation of hypochlorite, chlorate and oxygen during NaCl electrolysis from alkaline-solutions at an RuO_2/TiO_2 Anode. *Journal of Applied Electrochemistry* **1992,** *22* (4), 315-324.

(43) Bergmann, M. E. H.; Rollin, J.; Iourtchouk, T. The occurrence of perchlorate during drinking water electrolysis using BDD anodes. *Electrochimica Acta* **2009,** *54* (7), 2102-2107.

(44) Kraft, A.; Stadelmann, M.; Blaschke, M.; Kreysig, D.; Sandt, B.; Schroder, F.; Rennau, J. Electrochemical water disinfection - Part I: Hypochlorite production from very dilute chloride solutions. *Journal of Applied Electrochemistry* **1999,** *29* (7), 861-868.

(45) Szpyrkowicz, L.; Radaelli, M.; Daniele, S. Electrocatalysis of chlorine evolution on different materials and its influence on the performance of an electrochemical reactor for indirect oxidation of pollutants. *Catalysis Today* **2005,** *100* (3-4), 425-429.

(46) Szpyrkowicz, L.; Kaul, S. N.; Neti, R. N.; Satyanarayan, S. Influence of anode material on electrochemical oxidation for the treatment of tannery wastewater. *Water Research* **2005,** *39* (8), 1601-1613.

(47) Szpyrkowicz, L.; Kaul, S. N.; Neti, R. N. Tannery wastewater treatment by electro-oxidation coupled with a biological process. *Journal of Applied Electrochemistry* **2005,** *35* (4), 381-390.

(48) Blatchley, E. R.; Cheng, M. M. Reaction mechanism for vhlorination of urea. *Environmental Science & Technology* **2010,** *44* (22), 8529-8534.

(49) Kapalka, A.; Katsaounis, A.; Michels, N. L.; Leonidova, A.; Souentie, S.; Comninellis, C.; Udert, K. M. Ammonia oxidation to nitrogen mediated by electrogenerated active chlorine on Ti/PtO_x-IrO_2. *Electrochemistry Communications* **2010,** *12* (9), 1203-1205.

(50) Peez, G.; Saiz, J.; Ibanez, R.; Urtiaga, A. M.; Ortiz, I. Assessment of the formation of inorganic oxidation by-products during the electrocatalytic treatment of ammonium from landfill leachates. *Water Research* **2012,** *46* (8), 2579-2590.

(51) Fernandes, A.; Pacheco, M. J.; Ciriaco, L.; Lopes, A. Anodic oxidation of a biologically treated leachate on a boron-doped diamond anode. *Journal of Hazardous Materials* **2012,** *199*, 82-87.

(52) Deborde, M.; von Gunten, U. Reactions of chlorine with inorganic and organic compounds during water treatment - Kinetics and mechanisms: A critical review. *Water Research* **2008,** *42* (1-2), 13-51.

(53) Vlyssides, A.; Barampouti, E. M.; Mai, S.; Arapoglou, D.; Kotronarou, A. Degradation of methylparathion in aqueous solution by electrochemical oxidation. *Environmental Science & Technology* **2004,** *38* (22), 6125-6131.

(54) Canizares, P.; Paz, R.; Lobato, J.; Saez, C.; Rodrigo, M. A. Electrochemical treatment of the effluent of a fine chemical manufacturing plant. *Journal of Hazardous Materials* **2006,** *138* (1), 173-181.

(55) Lei, X. H.; Maekawa, T. Electrochemical treatment of anaerobic digestion effluent using a Ti/Pt-IrO_2 electrode. *Bioresource Technology* **2007,** *98* (18), 3521-3525.

(56) Bonfatti, F.; Ferro, S.; Lavezzo, F.; Malacarne, M.; Lodi, G.; De Battisti, A. Electrochemical incineration of glucose as a model organic substrate - II. Role of active chlorine mediation. *Journal of the Electrochemical Society* **2000,** *147* (2), 592-596.

(57) Mohan, N.; Balasubramanian, N.; Basha, C. A. Electrochemical oxidation of textile wastewater and its reuse. *Journal of Hazardous Materials* **2007,** *147* (1-2), 644-651.

(58) *Energy demands on water resources: Report to congress on the interdependency of energy and water*; United States Department of Energy: Washington D.C., 2006.;

http://www.sandia.gov/energy-water/docs/121-RptToCongress-EWwEIAcomments-FINAL.pdf.

(59) Li, M.; Feng, C. P.; Zhang, Z. Y.; Shen, Z. L.; Sugiura, N. Electrochemical reduction of nitrate using various anodes and a Cu/Zn cathode. *Electrochemistry Communications* **2009,** *11* (10), 1853-1856.

(60) Kim, B. R. Effect of ammonia on COD analysis. *Journal Water Pollution Control Federation* **1989,** *61* (5), 614-617.